COMPDYN 2015
5th ECCOMAS Thematic Conference on
Computational Methods in Structural Dynamics and Earthquake Engineering
M. Papadrakakis, V. Papadopoulos, V. Plevris (eds.)
Crete Island, Greece, 25–27 May 2015

SEISMIC RETROFIT DECISION-MAKING OF BRIDGES BASED ON LIFE-CYCLE COST CRITERIA

Hossein Ebrahimian[1], Fatemeh Jalayer[2], and Gaetano Manfredi[3]

[1] Post-doctoral Researcher
Dep. of Structures for Engineering and Architecture, University of Naples Federico II, Naples, Italy
e-mail: ebrahimian.hossein@unina.it

[2] Associate Professor
Dep. of Structures for Engineering and Architecture, University of Naples Federico II, Naples, Italy
fatemeh.jalayer@unina.it

[3] Professor
Dep. of Structures for Engineering and Architecture, University of Naples Federico II, Naples, Italy
gamanfre@unina.it

Keywords: Seismic Retrofit of Bridges, Retrofit Decision-making, Life-Cycle Cost Criteria, Time-dependent Risk, Limit State Probability.

Abstract. *In a decision-making framework within the context of performance-based design, life-cycle cost can be regarded as a suitable benchmark performance variable to quantify and measure performance objectives for a set of (discrete) limit states. Life-cycle cost criteria is identified as an economic term expressed in monetary units; it accounts for the initial construction costs, the repair costs taking into account also the loss of revenue due to down time, and finally the maintenance cost. The expected life-cycle cost is used for retrofit design of an existing reinforced concrete bridge infrastructure that is located in south of Italy. The retrofit design involves decision-making between a set of viable rehabilitation schemes, which mainly isolate the simply-supported bridge deck from the pier cap or force the deck to have a uniform displacement along its longitudinal direction. The proposed methodology for life-cycle cost assessment takes the advantage of a closed- and analytic-form approximation in order to take into account the time-varying profile of the probability of exceeding a set of structural limit states. The presented procedure can be effectively used for screening among alternative proposed upgrading strategies while satisfying prescribed reliability-based criteria. The optimal solution is highlighted based on the minimization of the life-cycle cost.*

1 INTRODUCTION

In the context of performance-based design, several performance objectives (e.g., minimize initial cost of construction, ensure life-safety in case of extreme and rare events) can be considered for a set of discrete limit states. In order to implement the performance objectives in a decision making framework, it is desirable to quantify and measure these objectives in terms of a common benchmark variable. The life-cycle cost has been proposed by many researchers (see e.g. [1-7]) as a suitable benchmark performance variable. Life-cycle cost, which is historically identified as an economic term expressed in monetary units, accounts for initial costs of construction of facility, the regular costs of its maintenance and its functionality over time, loss of revenue in case of damage, re-pair / replacement costs, social losses including eventual loss of life and end-of-life recycling costs. The evaluation of life-cycle cost is subjected to several sources of uncertainty, such as the occurrence and the intensity of future earthquake events, the structural resistance and the service life itself. Life-cycle cost is generally evaluated in terms of its expected value over the life-time of the infrastructure.

The present study aims to apply the life-cycle cost criteria to retrofit design of an existing reinforced concrete (RC) bridge with simply-supported decks built in the 1970s and located in the Campania Region, south Italy. The retrofit design involves decision making between a set of viable options which can be evaluated and compared in terms of their corresponding life-cycle cost and subjected to reliability constraints. In particular, for each upgrade option, the corresponding life-cycle cost is evaluated by calculating in monetary terms, the direct cost of the installation of the upgrade solution, the maintenance cost of the upgraded system, the re-pair/replacement costs in case of damage. After the low-cost option is identified among the set of retrofit schemes, the structural reliability for the corresponding upgraded infrastructure needs to be verified against an acceptable threshold.

The methodology for calculating the life-cycle cost takes into account the time-varying profile of the probability of exceeding a set of structural limit states. Thus, in the first step, a procedure is proposed for calculating the time-dependent probability of exceeding different structural limit states given a sequence of major seismic events. It takes advantage of a recently developed framework by the authors which was proposed for post-mainshock risk assessment [8-10]. Later, a closed- and analytic-form approximation to the time-dependent limit state probability is derived (see also [10]). The calculated time-dependent limit state probabilities based on the closed-form expression are then used in order to estimate the expected life-cycle cost for each retrofit option considered.

For the simplicity of calculations, the three-dimensional (3D) model of the case-study bridge is subjected to ground motions in its longitudinal direction. Five alternative schemes are adopted for rehabilitation of the bridge. They aim mainly at improving the global behavior of bridge deck by using friction pendulum isolators and/or force the deck to have a uniform displacement along its longitudinal direction. The optimal solution is highlighted based on the minimization of the life cycle cost satisfying the acceptable reliability-based criteria.

2 METHODOLOGY

The objective of this methodology is to evaluate the expected life-cycle cost for a bridge that is subjected to seismic actions during its life-time neglecting the effect of aging (given the fact that this methodology is used for optimal decision-making and not for assessment purposes). First, a method is proposed in order to calculate the time-dependent risk in terms of the probabilities corresponding to the exceedance of desired (discrete) limit states during the entire lifetime of the bridge (considering the sequence of seismic events that may take place during the bridge life cycle). It implements the methodology presented primary in [6, 8], and

further developed in [9]. Subsequently, to facilitate the estimation of time-dependent limit state exceedance probability, a simple closed-form and analytical approximation is derived. It employs the standard tools in risk assessment such as the fragility curve for the intact structure and takes into account that the bridge is going to be repaired before the next events takes place. These results are directly used within the calculation of the repair cost.

Accordingly, the expected life-cycle cost is calculated by taking into account the initial construction costs, the repair costs taking into account also the loss of revenue due to down time, and finally the maintenance cost. The calculations involved in this methodology are based on a set of assumption described in the following section. The presented probability-based methodology for evaluation of the expected life-cycle cost herein can be effectively used for screening among various proposed upgrading strategies while satisfying prescribed reliability constraints.

2.1 The Set of Assumptions

The following assumptions are adopted herein:

1. Once a major seismic event (i.e., the one with magnitude greater than a prescribed threshold) hits the bridge, the decision follows the immediate shutdown of the bridge and repairing of the infrastructure.
2. The repair operation is supposed to restore the infrastructure back to its intact initial state.
3. The time of repair, which is also equal to the down-time for the infrastructure, depends only on the state of the damaged bridge. It is likely that major seismic events take place while the bridge is under repair.
4. The bridge is going to be replaced / recycled while the following conditions arise: a) the infrastructure goes beyond the defined ultimate limit states, and b) the cost of repair operations exceeds the replacement costs.
5. The sequence of major seismic events taking place does not include the clustering of seismic events (i.e., aftershocks); previous works by the authors has focused on the clustered events (see [8-10]).
6. The effect of aging is not considered.

2.2 Calculation of Time-dependent Limit State Probability

Assume that $\mathbf{I}_1$ stands for the information as follows: t denotes the life time of the bridge (generally defined in unit of year); N_{ce} represents the maximum number of critical seismic events that can take place during the time interval $[0,t]$ and have magnitude M within the range $M_l \leq M \leq M_u$ (M_l is the lower magnitude and M_u defines the upper-bound magnitude). The probability of first-excursion for the desired limit state LS given $\mathbf{I}_1$, denoted by $P(LS|\mathbf{I}_1)$ can be expanded by using Total probability Theorem [11]:

$$P\left(LS \mid \mathbf{I}_1\right) = \sum_{n=1}^{N_{ce}} P\left(LS \mid n, \mathbf{I}_1\right) P\left(n \mid \mathbf{I}_1\right) \tag{1}$$

where $P(LS|n,\mathbf{I}_1)$ is the probability of exceeding the limit state LS for the first time given that exactly $n=1{:}N_{ce}$ events take place and $\mathbf{I}_1$; $P(n|\mathbf{I}_1)$ is the probability that exactly n events with $M_l \leq M \leq M_u$ take place during t. Assuming that the earthquake occurrence in the life-time of the bridge infrastructure is expressed by a stationary Poisson probability mass function, $P(n|\mathbf{I}_1)$ can be expressed as:

$$P(n \mid \mathbf{I}_1) = \frac{(\nu t)^n e^{-\nu t}}{n!} \tag{2}$$

where ν is the annual rate of seismicity (i.e., annual rate of occurrence of events with $M_l \leq M \leq M_u$). The best-estimate for N_{ce} in Eq. (1) can be adopted herein as the expected value plus two standard deviations ($N_{ce} \approx \nu t + 2[\nu t]^{1/2}$) for the distribution $P(n|\mathbf{I}_1)$ provided by the Poisson model. The term $P(LS|n,\mathbf{I}_1)$ in Eq. (1) can be calculated by taking into account the set of mutually exclusive and collectively exhaustive (MECE) events that the *LS* first-excursion is taken place at one and just one of the previous events (see [6-10]):

$$P\left(LS \mid n, \mathbf{I}_1\right) = P\left(C_1 + \overline{C}_1 C_2 + \overline{C}_1 \overline{C}_2 C_3 + \ldots + \overline{C}_1 \overline{C}_2 \ldots \overline{C}_{n-1} C_n\right) \tag{3}$$

where C_k, k=1:n, is defined by the following statement:

$$\begin{cases} C_k \equiv LS \text{ first-excursion after } k\text{th event} \\ \overline{C}_k \equiv LS \text{ not exceeded after } k\text{th event (read as NOT } C_k) \end{cases} \tag{4}$$

The authors have shown that $P(LS|n,\mathbf{I}_1)$ in Eq. (3) can be written as (see Appendix of [9]):

$$\begin{aligned} P\left(LS \mid n, \mathbf{I}_1\right) &= \sum_{k=1}^{n} \left(P\left(C_k \mid \overline{C}_1 \overline{C}_2 \ldots \overline{C}_{k-1}, \mathbf{I}_1\right) \cdot \prod_{i=1}^{k-1} \left[1 - P\left(C_i \mid \overline{C}_1 \overline{C}_2 \ldots \overline{C}_{i-1}, \mathbf{I}_1\right)\right] \right) \\ &\triangleq \sum_{k=1}^{n} \left(\Pi_k \cdot \prod_{i=1}^{k-1} \left(1 - \Pi_i\right) \right) \end{aligned} \tag{5}$$

where Π_k denotes the probability of *LS* first-excursion due to the occurrence of the kth event given that the limit state has not exceeded in the previous (k-1) events and $\mathbf{I}_1$. For the sake of brevity, the conditioning information that the limit state first-excursion did not take place in the previous events together with $\mathbf{I}_1$ is expressed hereafter as $\mathbf{I}_2$. The probability term Π_k in Eq. (5) can further be expanded with respect to the ground motion intensity measure *IM*, as follows (see also [9]):

$$\Pi_k = \int_{\text{all } x} P\left(C_k \mid x, \mathbf{I}_2\right) p\left(x \mid \mathbf{I}_2\right) \mathrm{d}x = \int_{\text{all } x} \pi_k\left(x\right) \left[\frac{1}{\nu} \cdot \left| \frac{\mathrm{d}\lambda_{IM}\left(x\right)}{\mathrm{d}x} \right| \right] \mathrm{d}x = \frac{1}{\nu} \int_{\text{all } x} \pi_k\left(x\right) \left| \mathrm{d}\lambda_{IM}\left(x\right) \right| \tag{6}$$

where x specifies *IM* associated with the kth event; $\pi_k(x)$ is called *event-dependent* fragility for the kth event given $\mathbf{I}_2$ [9]. The set of event-dependent fragilities $\{\pi_n(x)|n=1{:}N_{ce}\}$ is estimated through a non-linear dynamic analysis procedure named *Sequential Cloud Analysis* which is discussed in Appendix of this paper. The probability $p(x|\mathbf{I}_2)$ is the likelihood of *IM* at x corresponding to the kth event (among the information within $\mathbf{I}_2$, the conditioning that the previous (k-1) events have not led to the exceedance of the limit state *LS* is ignored as it is already seen in calculating π_k); $p(x|\mathbf{I}_2)$ can be derived directly from the site-specific seismic hazard in terms of the mean annual rate of exceeding x, i.e. $\lambda_{IM}(x)$, as shown in Eq. (6) where $\mathrm{d}\lambda_{IM}(x)/\mathrm{d}x$ is the slope of the seismic hazard curve. In general, Π_k is solved using numerical integration by computing the product of the event-dependent fragility and the differential of the seismic hazard curve at discrete values x, adding the results from all x, and then multiplying by $1/\nu$.

Although $P(LS|\mathbf{I}_1)$ is estimated within the time-interval $[0,t]$, the first-excursion probability in the time interval $[0,t+\Delta t]$ denoted as $P(LS|t+\Delta t,\mathbf{I}_1)$ where Δt is a time increment, can be expressed as:

$$P\left(LS \mid t+\Delta t, \mathbf{I}_1\right) = P\left(LS \mid \mathbf{I}_1\right) + P\left(LS \mid [t, t+\Delta t], \mathbf{I}_1\right) \tag{7}$$

where the second term in Eq. (7) denotes the time-dependent limit state first-excursion probability in the time interval $[t, t+\Delta t]$, and equals [8]:

$$P\left(LS \mid [t, t+\Delta t], \mathbf{I}_1\right) = P\left(LS \mid t+\Delta t, \mathbf{I}_1\right) - P\left(LS \mid \mathbf{I}_1\right) \tag{8}$$

Thus, by setting Δt=1 year, the limit state first-excursion probability in one-year time interval $[t, t+1]$ can be attained.

2.3 A Closed-form Approximation to Time-dependent Limit State Probability

The term $P(LS|\mathbf{I}_1)$ in Eq. (1) is approximated with a closed-form analytic expression based on the methodology preliminary proposed in [10]. Assume that the set of probability terms $\{\Pi_k | k=1{:}n\}$ introduced in Eq. (5) is identical and equal to the time- and event-invariant function Π. Thus, $P(LS|n,\mathbf{I}_1)$ in Eq. (5) can be regarded as the sum of a geometric series:

$$P\left(LS \mid n, \mathbf{I}_1\right) = \Pi \cdot \sum_{k=1}^{n} \left(1-\Pi\right)^{k-1} = \Pi \cdot \frac{1-\left(1-\Pi\right)^{n}}{1-\left(1-\Pi\right)} = 1-\left(1-\Pi\right)^{n} \tag{9}$$

Substituting $P(LS|n,\mathbf{I}_1)$ from Eq. (9) and $P(n|\mathbf{I}_1)$ from Eq. (2) into $P(LS|\mathbf{I}_1)$ in Eq. (1), we have:

$$\begin{aligned} P\left(LS \mid \mathbf{I}_1\right) &= \sum_{n=1}^{N_{ce}} \left(1-\left(1-\Pi\right)^{n}\right) \cdot \frac{\left(\nu t\right)^{n} e^{-\nu t}}{n!} \\ &= \sum_{n=1}^{N_{ce}} \frac{\left(\nu t\right)^{n} e^{-\nu t}}{n!} - \sum_{n=1}^{N_{ce}} \left(1-\Pi\right)^{n} \cdot \frac{\left(\nu t\right)^{n} e^{-\nu t}}{n!} \end{aligned} \tag{10}$$

The first term in Eq. (10) equals the sum of the Poisson Probability Mass Function (PMF) terms starting from n=1. Knowing that the sum of the Poisson PMS terms starting from n=0 is equal to unity, the first term in Eq. (10) equals 1-exp(νt). Subsequently, Eq. (10) can be further simplified as follows:

$$\begin{aligned} P\left(LS \mid \mathbf{I}_1\right) &= \left(1-e^{-\nu t}\right) - e^{-\Pi \nu t} \sum_{n=1}^{N_{ce}} \frac{\left(\left(1-\Pi\right) \cdot \nu t\right)^{n} e^{-(1-\Pi)\nu t}}{n!} \\ &= \left(1-e^{-\nu t}\right) - e^{-\Pi \nu t}\left(1-e^{-(1-\Pi)\nu t}\right) \end{aligned} \tag{11}$$

As a result, the closed-form approximation to the time-dependent limit state probability $P(LS|\mathbf{I}_1)$ in Eq. (11) is derived as:

$$P\left(LS \mid \mathbf{I}_1\right) = 1-\exp\left(-\Pi \nu t\right) \tag{12}$$

The closed-form expression in Eq. (12) serves as a simple analytic equation for calculating the time-dependent *LS* first-excursion probability due a sequence of events. There are different proposals that can be drawn for Π, which can be defined based on the alternative decisions for the repair of the bridge system, as will be discussed in the next section.

Nevertheless, it is interesting to note that with reference to Eq. (6), k=1 denotes the occurrence of one event, where π_1 can be interpreted as the structural fragility for the intact bridge, and the limit state exceedance can be described by a homogenous Poisson process with rate λ_{LS}. Thus,

$$\Pi_1 = \frac{1}{\nu} \int_{\text{all}\,x} \pi_1(x) \left| \mathrm{d}\lambda_{IM}(x) \right| = \frac{\lambda_{LS}}{\nu} \tag{13}$$

In case of using $\Pi=\Pi_1$, the exceedance probability in Eq. (12) can be further expressed as:

$$P(LS \mid \mathbf{I}_1) = 1 - \exp(-\lambda_{LS} t) \tag{14}$$

which is respectively the standard and well-known equation of the probability of occurrence of at least one event in a period of time $[0,t]$, considering the fact that the occurrence of events are described by a homogenous Poisson process. In this method, it is assumed that the bridge is going to be repaired immediately after the occurrence of a major seismic event with a repair time, τ, that is assumed to be equal to zero. Thus, the limit state first-excursion becomes a Poisson process. As a convention for the rest of current paper, the calculation of time-dependent limit-state probability by employing Eq. (14) is addressed as "*Standard method*", and is denoted as $P(LS|\tau=0,\mathbf{I}_1)$.

In a research study conducted recently by the authors [10], the closed-form analytical expression was utilized for calculating the post-mainshock limit state probability. It was investigated the even using the fragility of intact structure in Eq. (12) leads to a very good agreement with the computationally extensive and time-consuming exact solution for limit state probability (as described in Section 2.2 by using the sequence of event-dependent fragilities). Therefore, in this study, the fragility of the intact bridge infrastructure, π_1, is used without emphasizing to provide any further comparison with the exact solution introduced in Section 2.2.

2.4 How does the decision for repair affect the probabilistic time-dependent risk formulation?

According to the assumptions previously made in Section 2.1, the objective here is to take into account the repairing decision (addressed in this paper as **R** *decision*) with a predefined repair time $\tau\neq0$. Accordingly, the time-dependent limit state probability by this approach is denoted herein as $P(LS|\tau,\mathbf{I}_1)$. Hence, the limit-state first excursion is not a Poisson process and depends on the history of events taken place. This decision is taken into account while estimating the set of probability terms $\{\Pi_n|n=1{:}N_{ce}\}$. For the Repair (**R**) decision, the set of probability terms $\{\Pi_{n,\mathbf{R}}|n=1{:}N_{ce}\}$ should further break down into the sum of two MECE events considering the fact that event n hits the intact (not damaged) bridge (denoted by D_0) or the damaged bridge (defined by D), as follows:

$$\Pi_{n,\mathbf{R}} = P(C_n, D_0 \mid \mathbf{I}_2) + P(C_n, D \mid \mathbf{I}_2) \tag{15}$$

As noted previously, $\mathbf{I}_2$ comprises the background information $\mathbf{I}_1$ and the information that the previous (n-1) events have not led to the first-excursion of the limit state *LS*. Eq. (15) expands as:

$$\Pi_{n,\mathbf{R}} = P(C_n \mid D_0, \mathbf{I}_2)\, p(D_0 \mid \mathbf{I}_2) + \sum_{j=1}^{n-1} P(C_n \mid D_j, \mathbf{I}_2)\, p(D_j \mid \mathbf{I}_2) \tag{16}$$

where $P(C_n|D_0,\mathbf{I}_2)$ is the conditional probability of *LS* first-excursion due to the occurrence of the nth event given that the bridge is repaired (back to its intact state) right before the last nth event takes place. As a result, this probability term equals Π_1 associated with the intact bridge infrastructure. Accordingly, $p(D_0|\mathbf{I}_2)$ is the probability that the bridge is repaired before occurrence of the nth event, which reveals that the inter-arrival time (IAT) between the last subse-

quent events, i.e. nth and (n-1)th events, is greater than the repair time τ associated with the limit state LS. Thus, $p(D_0|\mathbf{I}_2)$ is the probability that IAT> τ which can be expressed as an Exponential distribution equal to exp(-$\nu\tau$). Consistently, $P(C_n|D_j,\mathbf{I}_2)$ can be interpreted as the LS first-excursion due to the nth event given that the damaged bridge is already subjected to j=1:n-1 seismic events while it have been under repair (the information extracted from $\mathbf{I}_2$ is that the previous j events have not led to the first-excursion of limit state LS). Hence, this probability term is identical to Π_{j+1}. In addition, $p(D_j|\mathbf{I}_2)$ is the probability of experiencing exactly j events (before the last nth event take place) while the bridge is being under repair (i.e., for all of the preceding j events, IAT< τ and the bridge became intact before jth event); hence, there are j independent and exponentially distributed probabilities that the IAT<τ, each can be expressed as 1-exp(-$\nu\tau$) in addition to the probability exp(-$\nu\tau$). As a result, Eq. (16) can be re-written as:

$$\Pi_{n,\mathbf{R}} = \Pi_1 e^{-\nu\tau} + \sum_{j=1}^{n-1} \Pi_{j+1}\, e^{-\nu\tau}\left(1-e^{-\nu\tau}\right)^j \tag{17}$$

With reference to Eq. (17), Π_1 is calculated from Eq. (13), while Π_{j+1} should be estimated from Eq. (6) using the event-dependent fragility π_{j+1}. However, in case of directly using the closed-form expression proposed in Eq. (12) for time-dependent limit state probability, proper assignment should be given to Π. In this case, one can set Π_{j+1}=Π_1, and directly calculate $\Pi_{2,\mathrm{R}}$ to be used as Π. Nevertheless, it would be much more convenient if one uses the so-called damaged bridge (i.e. Π_2) and assign it to all Π_{j+1}, and then set Π=$\Pi_{2,\mathrm{R}}$ in Eq. (12). The time-dependent limit-state probability by considering the repair, **R**, decision is called herein as "**R** *decision*".

2.5 Expected Life-Cycle Cost

The expected life-cycle cost given the information $\mathbf{I}_1$ can be expressed as [1]:

$$\mathbb{E}[C \mid \mathbf{I}_2] = C_0 + C_\mathrm{R} + C_\mathrm{M} \tag{18}$$

where C_0 is the initial construction or upgrade installation cost, C_R is the repair or replacement costs taking into account also the loss of revenue due to downtime, and C_M is the annual maintenance costs. The repair cost C_R can be calculated from the following equation:

$$\begin{aligned} C_\mathrm{R} &= \sum_t \sum_{ls=1}^{N_{LS}} LSC_{ls} \cdot e^{-\lambda_\mathrm{d} t}\left[P\left(LS_{ls} \mid [t,t+1],\mathbf{I}_1\right) - P\left(LS_{ls+1} \mid [t,t+1],\mathbf{I}_1\right)\right] \\ &= \sum_t \sum_{ls=1}^{N_{LS}} LSC_{ls} \cdot e^{-\lambda_\mathrm{d} t} \cdot \Delta P\left(LS_{ls} \mid [t,t+1],\mathbf{I}_1\right) \end{aligned} \tag{19}$$

where N_{LS} is the number of desired limit states ordered from the service up to the collapse, and ls, where ls=1:N_{LS}, accounts for the limit state under consideration; LSC_{ls} is the expected cost of restoring the bridge infrastructure from the lsth limit state LS_{ls} back to its intact state including eventual loss of revenue caused by interruption for repair operations; λ_d is the annual discount rate and exp(-$\lambda_\mathrm{d}t$) denotes the change in the monetary-based evaluations per time; $P(LS_{ls}|[t,t+1],\mathbf{I}_1)$ derived from Eq. (8) is the time-dependent first-excursion probability of limit state LS_{ls} in one-year for the time-interval [t,t+1]. The term $\Delta P(LS_{ls}|[t,t+1],\mathbf{I}_1)$ denotes the annual probability in the time interval [t,t+1] that the infrastructure is between the two subsequent limit states ls and ls+1; needless to say that for the collapse limit state (i.e., the last limit

state $ls=N_{LS}$), this probability differential ΔP becomes $P(LS_{N_{LS}}|[t,t+1],\mathbf{I}_1)$. It is also noteworthy that t starts from one as the relationship in Eq. (8) is meaningful for t_{life} starting from one.

The cost of maintenance C_M can be estimated as:

$$C_M = \int_0^{t_{life}} C_m e^{-\lambda_d t} dt = \frac{C_m}{\lambda_d}[1 - e^{-\lambda_d t_{life}}] \tag{20}$$

where C_m is the (constant) annual maintenance cost.

3 NUMERICAL EXAMPLE

The methodology described in Section 2 is applied to screening of alternative retrofit options associated with an existing bridge infrastructure in order to find the most suitable retrofit solution according to life cycle cost and reliability criteria.

3.1 Bridge Infrastructure Description

The case-study bridge examined in this study is a RC bridge built in the 1970s and located in the Campania Region, south Italy. It consists of six simply supported decks having independent spans of 41.00 meters, as illustrated in Fig. 1. It is worth mentioning that the bridge is representative of the Italian bridge inventory considering the fact that approximately 90% of the Italian highway bridges are represented by multi-span simply supported deck bridges (either with independent spans or with continuous cast in situ top slab above the piers) (see [12,13]).

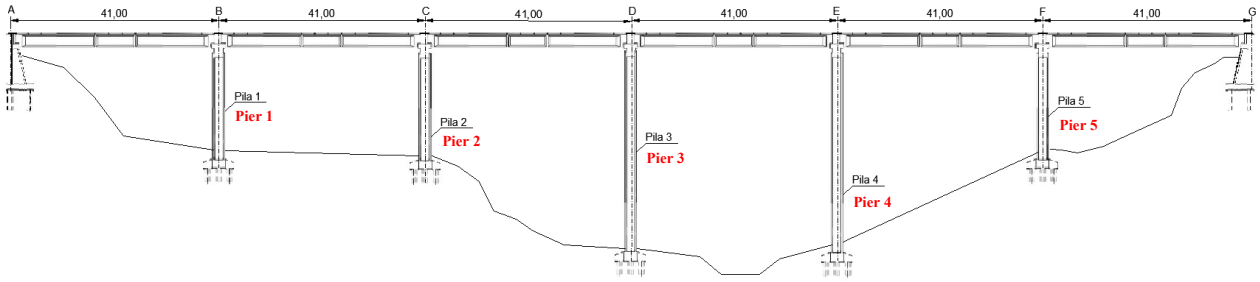

Figure 1: The longitudinal profile of the case-study bridge

The decks are supported by five pairs of box-type piers which are classified into two different types of cross section as shown in Fig. 2: the central piers (numbered as 3 and 4 in Fig. 1) which are approximately 40 m high, and the remaining tree piers defined with numbers 1, 2 and 5 in Fig. 1, with a height of around 20 m.

The simply-supported deck, whose cross section is illustrated in Fig. 3, consists of eight longitudinal beams with an upper cast-in-place slab of thickness 20 cm. The decks are supported on the cap-beams by means of elastomeric (neoprene) bearing supports. The abutments are seat-type, with neoprene bearing pads.

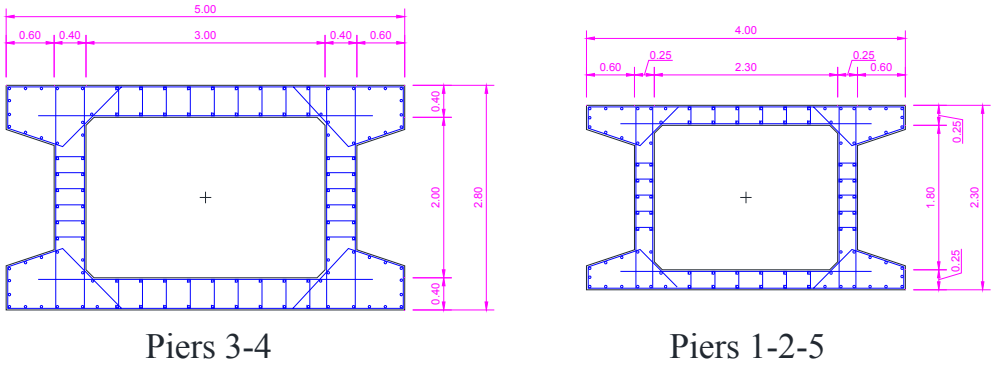

Figure 2: The cross section of piers

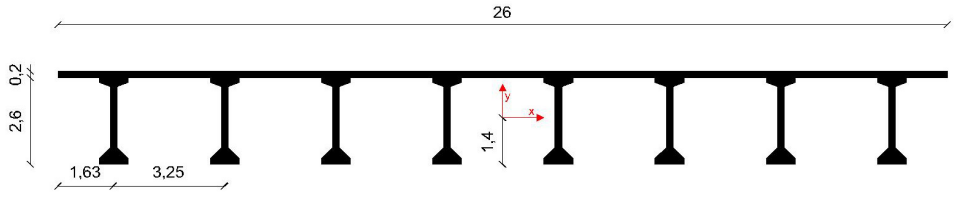

Figure 3: The cross section of simply-supported decks (dimensions are in meters)

3.2 Development of Bridge Model

The three-dimensional (3D) model of the bridge was created in the nonlinear finite element analytical program OpenSees [14], which provides an adequate element and material library for earthquake engineering applications. Illustrative descriptions of the nodal and element designations and boundary conditions corresponding to the spine-line model for the case-study bridge, with line elements located at the centroids of the cross-sections, are shown in Fig. 4. This figure serves as a representative model for a typical double pier and the deck above it as well as the abutment in both longitudinal and transverse directions, which is used as the OpenSees simulation model. The global directions are shown on this figure

In this figure, nodes are shown with hollow black circles. Individual components are included in this figure: (1) pair of piers considered as nonlinear components, (2) deck considered as a linear elastic component, (3) cap-beam shown as rigid element (RE), (4) bearing device defined with zero-length (denoted as *zeroLength*) elements, and (5) the seat-type abutment where the deck beam is seated on the abutment bearing pad defined with *zeroLength* element. It is noteworthy that the connection of the column bent to the pile cap is considered to be rigid for the case-study herein; hence, no pile-soil-structure interaction is taken into account. In addition, many features in the modeling of abutments and its interaction with the soil are neglected herein for simplicity. Important assumptions and main aspects of the modeling process of each individual component are described in the following subsections.

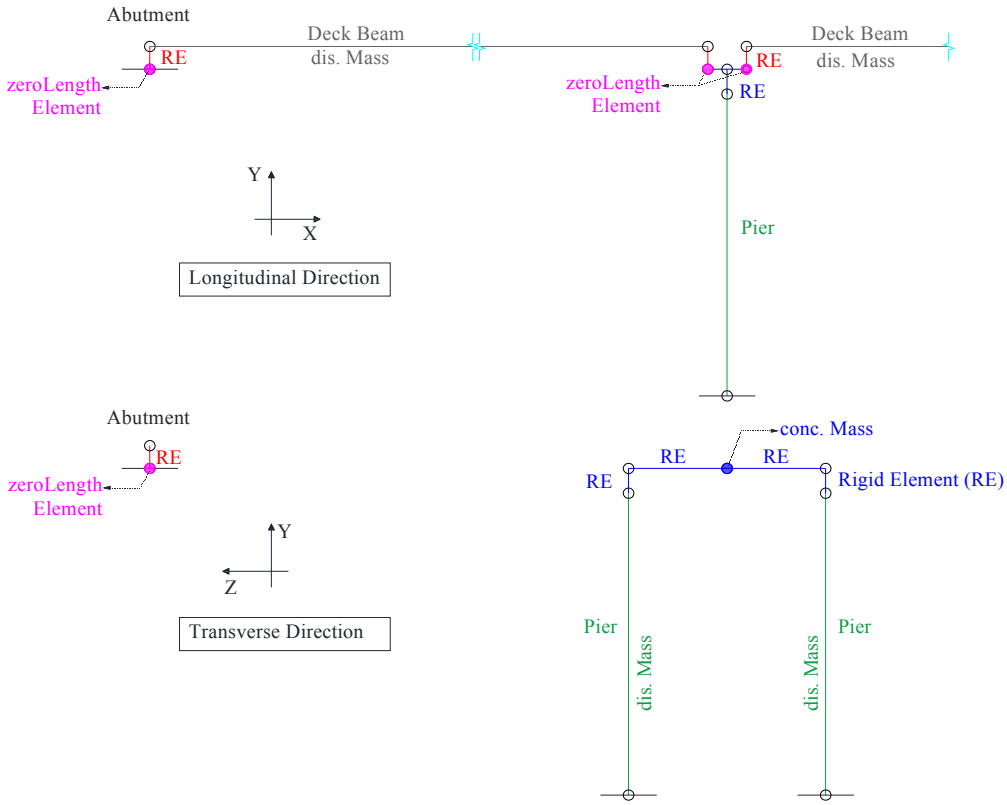

Figure 4: The cross section of simply-supported decks (dimensions are in meters)

3.2.1. Modeling of Deck

Simply-supported Decks are modeled using elastic beam-column elements, since flexural yielding of the deck during seismic response is not expected to take place. Although cracked section properties can obtain realistic values for the infrastructure's period and the seismic demands generated from the analyses, the effective moment of inertia of the deck beams, denoted as I_{eff} is set to that of the gross section (I_g). Needless to say that since all elements are modeled in the centerline of the bridge components (as mentioned earlier), it is required to consider the distance between the centroid of the deck-beam's cross-section (see Fig. 3) and the cap-beam's top. Instead of assigning a rigid joint offset to the deck beams, rigid beam elements (red RE elements in Fig. 4) are modeled which connect the deck beam to the bearing devices on the top of cap-beams. The material properties of deck members are defined subsequently.

3.2.2. Modeling of Cap-beam

A rigid beam element is used to represent the cap-beam, as shown by horizontal blue RE elements in Fig. 4. The cap-beam is connected by the elastomeric bearing supports to the superstructure.

3.2.3. Modeling of Piers

The main source of nonlinearity in this bridge model is reflected in its piers, where the evolution of column yielding and damage are expected under strong ground motions. Hence,

nonlinear force-based beam-column elements are used to represent the nonlinear behavior of piers in Opensees [14]. It is worth mentioning that in the distributed plasticity integration methods for force-based beam-column formulation (e.g. Gauss–Lobatto integration), it is not possible to represent both the spread of plasticity under hardening and member and section response under softening. Therefore, a new plastic hinge integration method based on modified two-point Gauss-Radau quadrature has been implemented which has the capability to overcome the difficulties that arise with Gauss–Lobatto integration for strain-softening behavior in force-based beam-column finite elements (for more details, see [15]).

Accordingly, the nonlinearity is assigned to both end of the piers within the plastic-hinge length and the interior portion of the beam-columns remains elastic. The analytical length of the plastic hinge in the piers is taken herein as the median of the equations suggested in [16], [17], and [18] respectively:

$$L_{\mathrm{p}} = 0.1L_{\mathrm{V}} + 0.17h + 0.24\frac{d_{\mathrm{bL}} f_y (\mathrm{MPa})}{\sqrt{f_c}\,(\mathrm{MPa})} \tag{21}$$

$$L_{\mathrm{p}} = 0.10L + 0.015 d_{\mathrm{bL}} f_y (\mathrm{MPa}) \cong 0.10L \tag{22}$$

$$L_{\mathrm{p}} = 0.08L + 0.022 d_{\mathrm{bL}} f_y (\mathrm{MPa}) \geq 0.044 d_{\mathrm{bL}} f_y \tag{23}$$

where L_{V} is the shear span (which is equal to the pier height L in longitudinal direction), h is the depth of the cross section, d_{bL} is the diameter of tension reinforcement, f_c is the concrete compressive strength (MPa), and f_y is the estimated mean value of steel yield strength (MPa) (see Section 3.2.5 for the material properties).

Fiber sections are assigned to the two pier sections (see Fig. 2) with two constitutive rules used simultaneously within a cross-section: (1) unconfined concrete, and (2) steel rebar. The concrete and reinforcing steel material properties are defined subsequently. In order to model the portion of the piers that are embedded in the cap-beam, a vertical blue RE elements are defined in the bridge model which connect pier's top to the centroid of the cap-beam (see Fig. 4). It should further be noted that the effect of bar-slip is not considered within the nonlinear modeling of bridge piers in this study. Slip of a pier's reinforcing bars in the base will cause rigid-body rotation of the pier, which cannot be accounted for in a flexural fiber analysis, where the column ends are assumed to be fixed.

3.2.4. Modeling of Abutments

A detailed description of abutment modeling with appropriate references can be found in [19]. In addition to the resistance of distributed bearing pads in both horizontal as well as vertical directions, there are important issues that should be considered in a comprehensive modeling of abutment. In the longitudinal direction of the bridge, the longitudinal stiffness of the zero-length element shown in Fig. 4 should also accounts for the gap between the deck and the abutment backwall as well as the active soil pressure behind the abutment backwall. Similarly, the transverse stiffness of the zero-length element should take into account the shear strength of the backfill soil behind the abutment backwall. In the vertical direction, in addition to the neoprene bearing pad stiffness in vertical direction, the abutment embankment stiffness should also be taken into account. All the assigned nonlinear zero-length elements should work only in compression.

Nevertheless, herein, a very simple abutment modelling is used, where the stiffness assigned to zero-length elements in three directions represents the stiffness of the neoprene bearing pads. The zero-length elements can work in tension and compression simultaneously;

this assumption can introduce a horizontal instability in the model when all the piers' chord rotations go beyond the rotational capacity associated with the maximum strength of piers.

3.2.5. Material Properties

For the reinforced concrete piers, the *Concrete04 UniaxialMaterial* of the OpenSees [14] material library is used in the modeling process which has the capability to consider the concrete model proposed by [20]. The following parameters were employed: unconfined concrete compressive strength f_c=20 MPa, the strain at maximum concrete stress ε_{c0}=0.002, the ultimate unconfined concrete strain ε_{c0}=0.005, and the concrete modulus of elasticity defined as follows:

$$E_C = 0.043 \cdot w^{1.5} \cdot \sqrt{f_c}\,(\text{MPa}) \cong 4700 \cdot \sqrt{f_c} = 21019\,\text{MPa} \tag{24}$$

where w is the unit weight of concrete. It is noteworthy that no tensile strength is considered for the concrete material. In addition, it is also recommended to assign unconfined and confined concrete material to the concrete cover and core of the pier section, respectively; nevertheless, this study assume an unconfined concrete material, as defined previously, for the whole pier section.

For the reinforcing steel material, a uniaxial Giuffre-Menegotto-Pinto steel material object with isotropic strain hardening, called *Steel02*, is used from OpenSees [14] material library. The advantage of this steel material is mainly the smooth translation of backbone curve from elastic range to plastic range, which leads to fewer convergence problems. For this purpose, the steel modulus of elasticity and the mean value of steel yield strength were set as E_s=200000 MPa and f_y=310 MPa, respectively. A strain-hardening ratio (ratio between post-yield tangent and initial elastic tangent) equal to 0.01 is considered.

3.2.6. Assignment of Masses and Damping

In order to achieve an accurate distribution of mass along the length of the bridge deck, a distributed mass is assigned to the elastic beam-column element of the deck beam which has the capability to construct a consistent mass matrix for these elements. In addition, a distributed mass along the height is also considered for the piers (see Fig. 4 for the assigned distributed masses). The mass of the cap-beam (i.e., those portions that are RE in Fig. 4) are concentrated at the mid-node of the cap-beam, as shown in Fig. 4.

Rayleigh damping is employed with a ξ=5% of critical damping coefficient in the first two modes of vibration (see [19, 21]). The classical damping matrix is a linear combination of the mass and stiffness matrices with the coefficients α_M and α_K, respectively [22]:

$$\alpha_M = 2\xi \frac{\omega_1 \cdot \omega_2}{\omega_1 + \omega_2},\ \alpha_K = 2\xi \frac{1}{\omega_1 + \omega_2} \tag{25}$$

where ω_1 and ω_2 are the frequencies associated with the first and second modes, respectively.

3.2.7. Shear Deformation in Pier Sections

In order to account for the shear deformation in piers due to shear force and torsional bending, section aggregator in OpenSees is used. To aggregate the shear deformation in the fiber section analysis of the piers, three elastic uniaxial materials are defined:

1. Two elastic materials with elastic shear stiffness equal to $G_C \times A_{vy}$ and $G_C \times A_{vz}$, which account for the shear deformation in two (local) perpendicular directions of the pier section y and z. G_C is the shear modulus of concrete; A_{vy} and A_{vz} are the effective shear area of the box-type piers which are less that the gross area of the pier, A_g.

2. One elastic material that accounts for the torsional deformation in the fiber section of the pier with the elastic torsional stiffness $0.20 \times G_C \times J_g$ where J_g is the polar moment of inertia of the cross-section of the pier. The reduction factor of 0.20 is used due to cracking of the pier cross-section [21].

It is to note that the shear deformation is calculated by assigning an elastic material. The use of more sophisticated models that account for nonlinear shear deformation is a plan for near future developments.

3.3 Alternative Retrofit Strategies

Five alternative schemes are adopted for rehabilitation of the case-study bridge infrastructure herein. They aim at improving the global behavior of bridge deck by using friction pendulum isolators and/or force the deck to have a uniform displacement along the longitudinal direction (see Table 1). More details about different retrofit options can be found in [23, 24]. The first-mode period, T_1, of the original (as-built) model of the bridge considering also the p-delta effect due to gravity loads is 2.46 sec. The first-more period of alternative retrofit options are outlined in Table 1.

Retrofit option	Description	Implementation in OpenSees (see Fig. 4)
ROD	The simply-supported decks are connected with chains	Impose the same longitudinal displacement to the adjacent nodes of the deck beams in both sides of the pier, T_1 = 1.99 sec
FP-R25	Friction Pendulum isolator with effective radius of concave sliding surface equal to 2.5 m and a Coulomb friction of 2%	Using Single Friction Pendulum Bearing Element together with a Coulomb friction model, T_1 = 3.20 sec
FP-R25-ROD	The combination of ROD and FP-R25	T_1 = 2.84 sec
FP-R31	Friction Pendulum isolator with effective radius of concave sliding surface equal to 3.1 m and a Coulomb friction of 5%	T_1 = 3.47 sec
FP-R31-ROD	The combination of ROD and FP-R31	T_1 = 3.15 sec

Table 1: Alternative retrofit strategies.

3.4 Definition of Limit States

In order to be consistent with recent studies on bridge infrastructures in Italy (see [12, 25]), two limit states (*LS*) or performance levels are considered: *damage* Limit State and *collapse* Limit State. The time-dependent limit state probabilities are evaluated based on both limit states. Each *LS* is associated with states of damage as summarized in Table 2.

According to this Table, *Damage LS* (denoted as DS) defines the condition of having limited structural damages in which it would be prudent to implement structural repairs. This may require traffic interruptions or the installation of temporary bracing systems. For this LS, the only DS that is considered is the pier yielding associated with ductility equal to one. Two important DSs that are not considered in this study are as follows: the bearings' failure when

the displacement exceeds the displacement capacity of the bearing device (it leads to the simple fall of the deck from the bearing seat); attainment of the active resistance of abutments (pulling action).

The *Collapse* LS takes into account the condition in which the extensive damages to bridge retain no margin against collapse. This implies that significant degradation has occurred in the stiffness and strength of the piers, and/or large displacements take place which might cause unseating of the decks. The infrastructure may be technically repairable, but costs could be very high and the closure of the bridge for long time is inevitable. The DSs considered for this limit state are: (1) pier collapse due to the attainment of its ultimate ductility or shear strength, (2) unseating of the deck due to the full loss of support from the cap-beam. It is to note that attainment of the passive resistance of abutments (pushing action) is also an important DS which is not taken into account in current study.

Limit Sate (LS)	State of Damage (SD)	Description
Damage (DS)	Pier flexural yielding	Pier chord rotation exceeds pier chord rotation at yielding, $\theta \geq \theta_y$
Collapse (CS)	Pier flexural capacity	Pier chord rotation exceeds pier chord rotation at collapse, $\theta \geq \theta_u$
	Pier shear capacity	Pier shear force exceeds pier shear resistance, $V \geq V_R(\theta)$
	Unseating of the deck	Deck displacement in the longitudinal direction is greater than the seat length

Table 2: Definition of Limit States.

According to Table 2, the allowable unseating length of the case=study bridge with reference to its original drawings is set to 60 cm. Moreover, Table 2 outlines the two thresholds considered for chord rotation of piers, namely θ_y and θ_u. These values are obtained directly from pushover analysis of single piers (i.e., base shear versus chord rotation) after applying the associated axial force due to gravity loads on each pier. Fig. 5 illustrates the actual pushover curves associated with two types of piers (i.e. piers 1-2-5 and piers 3-4, as shown in Fig. 2) in longitudinal (global X) direction. The onset of damage and collapse limit states are marked on the pushover curves in terms of the chord rotation. It is noteworthy that θ_y is marked by visual inspection on the pushover curve trend, while θ_u threshold is set to 20% drop in ultimate strength of the piers as denoted in [26].

The shear strength, V_R, is calculated by the provisions of [16] (see also [27]), that is commonly suggested for the assessment of existing buildings under cyclic loads. The shear strength is obtained from the following equation:

$$V_R = \frac{1}{\gamma_{\text{el}}}\left(V_N + V_C + V_W\right) \tag{26}$$

where

$$V_N = \frac{h-x}{2L_{\text{V}}} \cdot \min\left(N, 0.55 A_c \frac{f_c}{\gamma_c}\right) \tag{27}$$

$$V_C = \left[1 - 0.05\min\left(5, \mu_\Delta^{\text{pl}}\right)\right] \cdot \left[0.16\max\left(0.5, 100\rho_{\text{tot}}\right) \cdot \left(1 - 0.16\min\left(5, \frac{L_V}{h}\right)\right) \cdot \sqrt{\frac{f_c}{\gamma_c}} A_c\right] \quad (28)$$

$$V_W = \left[1 - 0.05\min\left(5, \mu_\Delta^{\text{pl}}\right)\right] \cdot \rho_w \cdot \frac{f_y}{\gamma_s} \cdot b_w \cdot z \quad (29)$$

where γ_{el}=1.15; x is the depth of the neutral axis at yielding; N is the is axial load; A_c is the area of the section; γ_c=1.50 is the partial safety factor of concrete; μ_Δ^{pl} is the plastic ductility factor which is equal to θ/θ_y-1; ρ_{tot} is the total longitudinal reinforcement ratio; ρ_w is the transverse reinforcement ratio; γ_s=1.15 is the partial safety factor of reinforcing steel; bw is the section width; z is the internal lever arm. In this study, A_c=$b_w \cdot d$ for the box-type section of the piers with the effective thickness b_w equal to two times the web thickness in the direction of loading, and d equal to the effective depth of the section.

The estimated values of the shear strength at the base of the two types of piers as a function of θ are also shown in Fig. 5 for the sake of comparison. It can be depicted that the shear strength is more critical in case of short piers (piers 1-2-5).

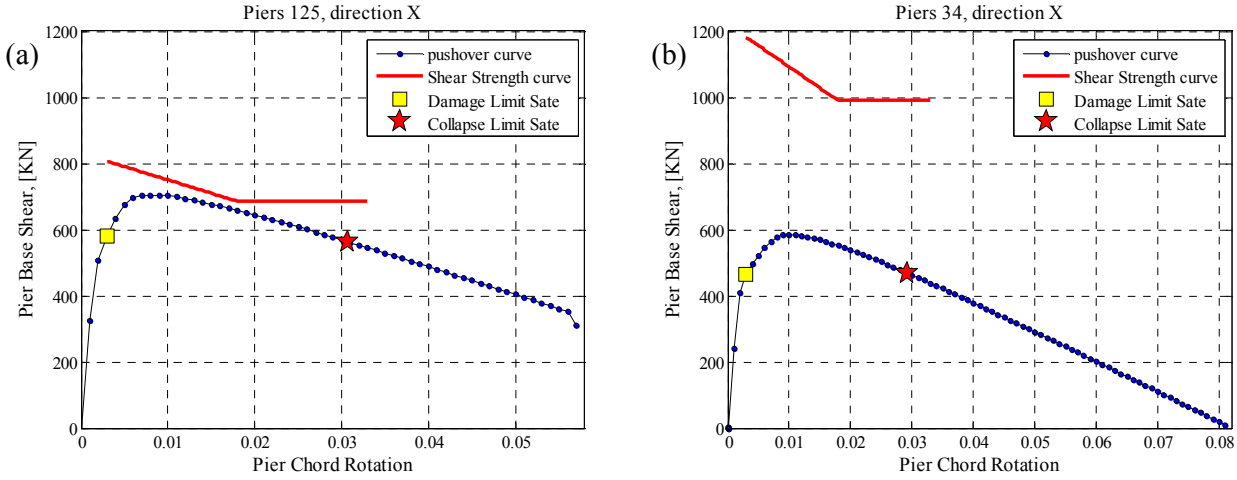

Figure 5: The pushover curve with the onset of both limit states associated with chord rotation marked on it, together with shear strength curve of the bridge piers (a) pier type 1-2-5, (b) pier type 3-4

3.5 Calculation of the structural performance variable Y_{LS}

The structural performance variable Y_{LS}, which is comprehensively defined in the Appendix of this paper as a time and history dependent performance variable, is generally the critical demand to capacity ratio. It is primarily introduced in [28], and further utilized in [9, 29]. It is recently used as a proper decision variable for assessing the existing bridge infrastructures in Italy [25, 30]. Since there are various SD's for a given limit state, Y_{LS} is capable of finding the critical situation while relating the structural behaviour at the component level to its global performance. For the case-study bridge system, a simple scheme of finding the weakest failure mode leads us directly to the global failure. Accordingly, for each limit state LS, Y_{LS} is obtained as:

$$Y_{LS} = \max_i^{N_{\text{SD}}} \max_j^{N_{\text{ele}}} \left(Y_{LS,ji}\right) \quad (30)$$

where N_{SD} is the states of damage for the considered LS, N_{ele} is the number of components taking part in the ith SD, and $Y_{LS,ji}$ is the value of Y_{LS} for the jth component of ith SD. Accordingly, in case of damage limit state, N_{SD}=1 and j=1:6 (as there exists 6 piers). Consequently, for the collapse limit state, N_{SD}=3 (i.e. i=1:3), where i=1:2, j=1:6 correspond to the pier flexural and shear capacities; nevertheless, i=3 denotes the SD corresponding to unseating of the deck with j=1:12 since the displacements at start and end nodes of the 6 simply-supported deck beams should be simultaneously monitored (see Fig. 1).

3.6 Selected Suite of Ground-motion Records

For performing the cloud analysis, a set of 25 European (especially Italian) strong ground motion records are selected from the NGA-West2 database [31], and listed in Table 3. This suite of selected records covers a wide range of magnitudes from 5.50 up to 7.51, and closest distance to ruptured area (R_{RUP}) up to 16 km, as illustrated in Fig. 6(a). This set of ground motions is chosen without emphasizing on detailed record selection which is not a primary focus in this study. The main concern, herein, is to provide a proper cloud response that cover the range of Y_{LS} from lower values to values higher than 1.

The associated spectral shapes are shown in Fig. 6(b). With reference to Table 3, nine records out of 25 are identified as pulse-like based on the algorithm proposed in [32], which can acquire pulses at arbitrary orientations in multi-component ground motions. The outlined pulse periods in Table 3 are obtained from the extracted pulses in the direction of the strongest observed pulse. It is to note that pulses are often found in other orientations due to complex geometry of a real fault; thus, the velocity pulse can be present in orientations other than the computed fault-normal orientation. The spectral accelerations of the nine pulse-like records are shown in Fig. 6(b) with bold lines. In order to draw a point of comparison, the uniform hazard spectra (UHS) for two hazard levels of 10% and 5% exceedance in 50 years are also illustrated on Fig. 6(b). It reveals the appropriateness of the selected set of records which provides a good variability around the UHS (although selecting spectrum compatible records has not been an objective herein).

3.7 Seismicity of the Site

The bridge's site with the coordinate [41.0264N, 14.795E] is located in the Campania region in the boundary of seismic zones 927 and 928, based on the Italian Seismogenic Zonation (ZS9) [33]. Fig. 7(a) shows the seismogenic zonation ZS9 with different zones identified on it; it can be seen that the desired sire is surrounded by the seismic zones 923, 924, 925, 926, 927 and 928, separately indicated in Fig. 7(b). The key seismicity parameters of each zone are outlined in Table 4.

Based on the seismicity data of each zone, a simplified site-specific probabilistic seismic hazard analysis (PSHA) is performed on the bridge site using the MATHAZARD [34]. The Sabetta and Pugliese 1996 attenuation relation [35] is chosen because of its wide use in Italy, and consistency with the INGV hazard maps (Istituto Nazionale di Geofisica e Vulcanologia, Progetto INGV-DPC S1, http://esse1.mi.ingv.it).

NGA Record Number	Earthquake Name	Station Name	Horizontal Component	Magnitude	Closest distance to the ruptured area, R_{RUP} (km)	Fault mecha-nism	NEHRP Site Classification	Lowest Usable Frequency (Hz)	Strongest Pulse Period (sec)
125	Friuli, Italy-01	Tolmezzo	2	6.5	15.82	Reverse	C	0.1625	
126	Gazli, USSR	Karakyr	1	6.8	5.46	Reverse	D	0.1625	
132	Friuli, Italy-02	Forgaria Cornino	2	5.91	14.75	Reverse	C	0.1875	
139	Tabas, Iran	Dayhook	2	7.35	13.94	Reverse	C	0.25	
143	Tabas, Iran	Tabas	2	7.35	2.05	Reverse	B	0.1	6.19
156	Norcia, Italy	Cascia	2	5.9	4.64	Normal	C	0.25	
285	Irpinia, Italy-01	Bagnoli Irpinio	2	6.9	8.18	Normal	C	0.1125	1.71
292	Irpinia, Italy-01	Sturno (STN)	2	6.9	10.84	Normal	C	0.1125	3.27
300	Irpinia, Italy-02	Calitri	2	6.2	8.83	Normal	C	0.1625	
313	Corinth, Greece	Corinth	2	6.6	10.27	Normal-Oblique	C	0.25	
821	Erzican, Turkey	Erzincan	1	6.69	4.38	Strike-Slip	D	0.1125	
1158	Kocaeli, Turkey	Duzce	2	7.51	15.37	Strike-Slip	D	0.1	
1176	Kocaeli, Turkey	Yarimca	1	7.51	4.83	Strike-Slip	D	0.0875	4.95
1602	Duzce, Turkey	Bolu	2	7.14	12.04	Strike-Slip	D	0.0625	0.88
1605	Duzce, Turkey	Duzce	2	7.14	6.58	Strike-Slip	D	0.1	5.94
1633	Manjil, Iran	Abbar	2	7.37	12.55	Strike-Slip	C	0.13	
4040	Bam, Iran	Bam	1	6.6	1.7	Strike-Slip	C	0.0625	2.02
4352	Umbria Marche, Italy	Nocera Umbra	2	6	8.92	Normal	C	0.875	
4367	Umbria Marche (aftershock 1), Italy	Nocera Umbra	2	5.5	9.33	Normal	C	0.75	
4451	Montenegro, Yugo.	Bar-Skupstina Opstine	2	7.1	6.98	Reverse	C	0.1625	1.44
4456	Montenegro, Yugo.	Petrovac - Hotel Olivia	1	7.1	8.01	Reverse	C	0.375	
4480	L'Aquila, Italy	L'Aquila - V. Aterno - Centro Valle	1	6.3	6.27	Normal	C	0.0375	1.07
4481	L'Aquila, Italy	L'Aquila - V. Aterno -Colle Grilli	1	6.3	6.81	Normal	C	0.05	
4509	L'Aquila (aftershock 1), Italy	L'Aquila - V. Aterno -Colle Grilli	1	5.6	14.95	Normal-Oblique	C	0.125	
4510	L'Aquila (aftershock 1), Italy	L'Aquila - V. Aterno - Centro Valle	1	5.6	14.81	Normal-Oblique	C	0.1125	

Table 3: The suite of strong ground-motion records used in this study

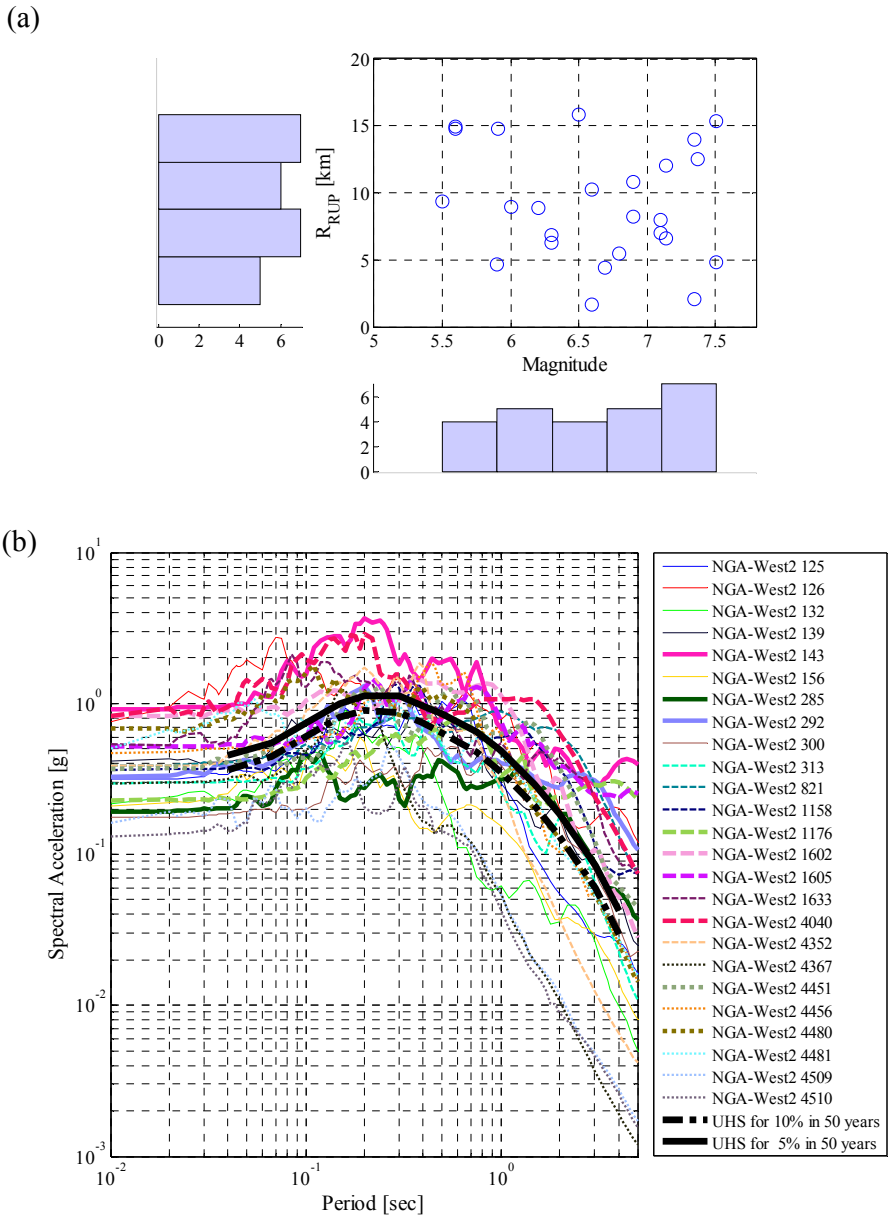

Figure 6: (a) Scatter diagram for the suite of records (Table 3) showing its range of magnitude and closest distance to ruptured area (R_{RUP}), (b) the spectral shape for the suite of records

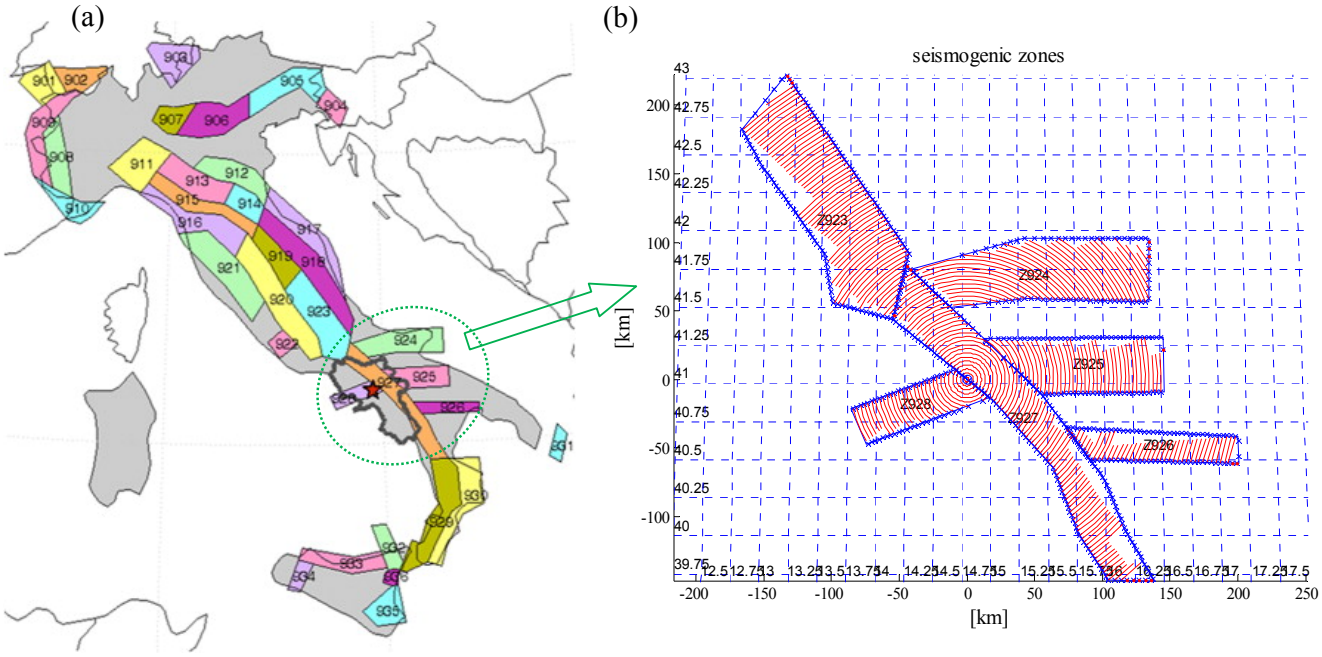

Figure 7: (a) The Italian seismogenic zonation ZS9 with different zones identified, the Campania region highlighted by a gray polyline, and the site of interest is schematically indicated by a pentagram (extracted from [36]), (b) the seismogenic zones surrounding the bridge site

Zone	Seismicity rate ν	Richter b-value	lower magnitude M_l	upper magnitude M_u
923	0.14	1.05	4.76	7.06
924	0.13	1.04	4.76	6.83
925	0.17	0.67	4.76	6.83
926	0.10	1.28	4.76	6.14
927	0.43	0.74	4.76	7.06
928	0.21	1.04	4.76	5.91

Table 4: Parameters of the ZS9 seismic zones surrounding the bridge site.

It is apparent that the selection of a suitable *IM* for representing ground motion uncertainty is a major concern and challenging issue that has to be addressed properly. The stronger is the correlation between the predicted Y_{LS} and the adopted *IM*, the more accurate will be the result of the limit state probabilities. This issue becomes more sensitive in the presence of various retrofit strategies, which are mainly isolation-type rehabilitation schemes. Nevertheless, this is currently not the major concern herein; thus, we opted to use the more simple and well-known *IM*s composed of peak ground acceleration (*PGA*), peak ground velocity (*PGV*), and spectral acceleration at the first-mode period of the bridge, $Sa(T_1)$.

Fig. 8 illustrates the site-specific PSHA in terms of the mean annual rate of exceedance for three aforementioned *IM*s, which was denoted in Section 2 as λ_{IM}. In Fig 8(a, b), the mean rate of exceedance in terms of *PGA* and *PGV* are shown respectively for each of the individu-

al zones as well as for their combination. However, in Fig. 8c, combined PSHA for $Sa(T_1)$ is shown for a range of periods.

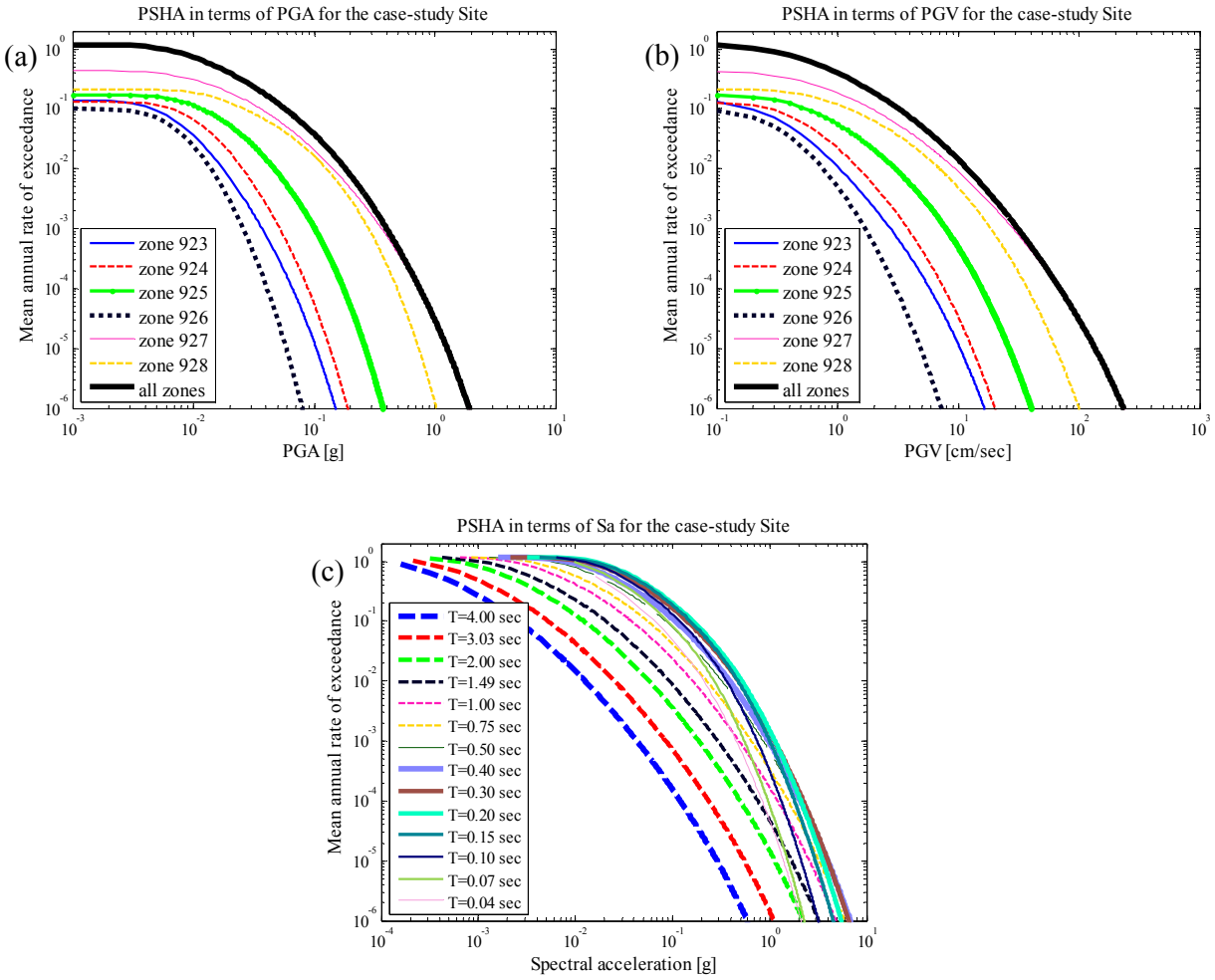

Figure 8: The site-specific seismic hazard results for (a) PGA, (b) PGV, and (c) $Sa(T_1)$

3.8 Estimating the time-dependent limit state probability $P(LS|\mathbf{I}_1)$

This section provides an objective description for calculating the time-dependent limit state probabilities $P(LS|\tau=0,\mathbf{I}_1)$ (denoted in Section 2.3 as *Standard method*) and $P(LS|\tau,\mathbf{I}_1)$ (defined in Section 2.4 as **R** *decision*) for the two desired limit states (see Table 2). The framework described in Section 2 is applied step-by-step to the case-study bridge infrastructure retrofitted with five different schemes outlined in Table 1. Nonetheless, it is worth mentioning that this study aims to use the simple analytic closed-form expression derived in Section 2.3 for estimating the limit state probability $P(LS|\mathbf{I}_1)$. As further explained in Section 2.3, the comparison between the results extracted from the closed-form expression with the exact solution proposed in Section 2.2 in not performed herein.

Step (1): Derive the fragility of the intact infrastructure π_1 based on the Sequential Cloud Analysis methodology described in Appendix. In order to perform this operation, the bridge infrastructure is subjected to the set of ground-motion records outlined in Table 3. In this

study, the records are applied only in the longitudinal direction of the bridge (i.e. bi-directional analysis of the bridge infrastructure is not performed herein). The results of non-linear dynamic analysis in terms of Y_{LS} are calculated based on the methodology described in Section 3.5. The cloud data, which consist of the *IM* of each record and the associated Y_{LS}, are consequently extracted. Fig. 8 illustrates the cloud regressions associated with Y_{CS} vs. *IM* for the Collapse limit state (CS) based on the three different *IM*s considered, respectively. The cloud data corresponding to the original bridge and the five proposed rehabilitation schemes are shown. It can be observed that the cloud data tend to cover the range of Y_{CS} from small values up to $Y_{CS}>1$ (the line corresponds to $Y_{CS}=1$ is marked on each figure). Moreover, the specific SD that has caused Y_{DS} based on Eq. (30) is assigned by a representative color as shown in the title of each regression plot.

The suitability of one *IM* with respect to another could be evaluated in terms of the average difference in information provided about the predicted Y_{LS}. To accomplish this task, a measure called *Relative Sufficiency Measure* (RSM) proposed in [37] is used herein. The RSM of IM_1 with respect to IM_2, denoted as $I(Y_{LS}|IM_2|IM_1)$, quantifies on average how much more information IM_1 relays to Y_{LS} about the ground motion with respect to IM_2. The RSM herein is calculated in an approximate manner (see [37, 38] and for the corresponding expression). If $I(Y_{LS}|IM_2|IM_1)$, measured in bits of information, is positive, this means that on average IM_2 provides more information about Y_{LS} than IM_1; hence, IM_2 is more sufficient than IM_1. Similarly, if $I(Y_{LS}|IM_2|IM_1)$ is negative, IM_2 is less sufficient than IM_1. The reference intensity (i.e., IM_1) is taken to be $Sa(T_1)$, and the RSM is measured for the other two candidate *IM*s (i.e. *PGA* and *PGV*) relative to $Sa(T_1)$, as summarized in Table 5 for both limit states, DS, and CS, and different bridge models.

Limit state	RSM $IM_1=Sa(T_1)$	Bridge Model					
		original	ROD	FP-R25	FP-R25-ROD	FP-R31	FP-R31-ROD
DS	$IM_2=PGA$	-1.72	-2.09	-1.20	-1.14	-1.30	-1.64
	$IM_2=PGV$	-0.75	-1.15	-0.28	-0.26	-0.38	-0.50
CS	$IM_2=PGA$	-0.81	-1.18	-0.82	-0.92	-0.57	-0.76
	$IM_2=PGV$	-0.24	-0.52	-0.15	-0.20	-0.07	-0.12

Table 5: RSM for *IM*s of *PGA* and *PGV* relative to $Sa(T_1)$ for both limit states DS and CS and different bridge models

With reference to Table 5, it can be concluded that $Sa(T_1)$ is the more efficient compared to *PGA* and *PGV*. Nevertheless, *PGV* is still more informative with respect to *PGA* for various retrofit alternatives of the case-study bridge.

The fragility curves for both limit states and for different bridge models can directly be calculated from the cloud regression data (as explained in the Appendix). Fig. 10 illustrates the fragility curves of various retrofit options based on desired *IM*s and for both limit states.

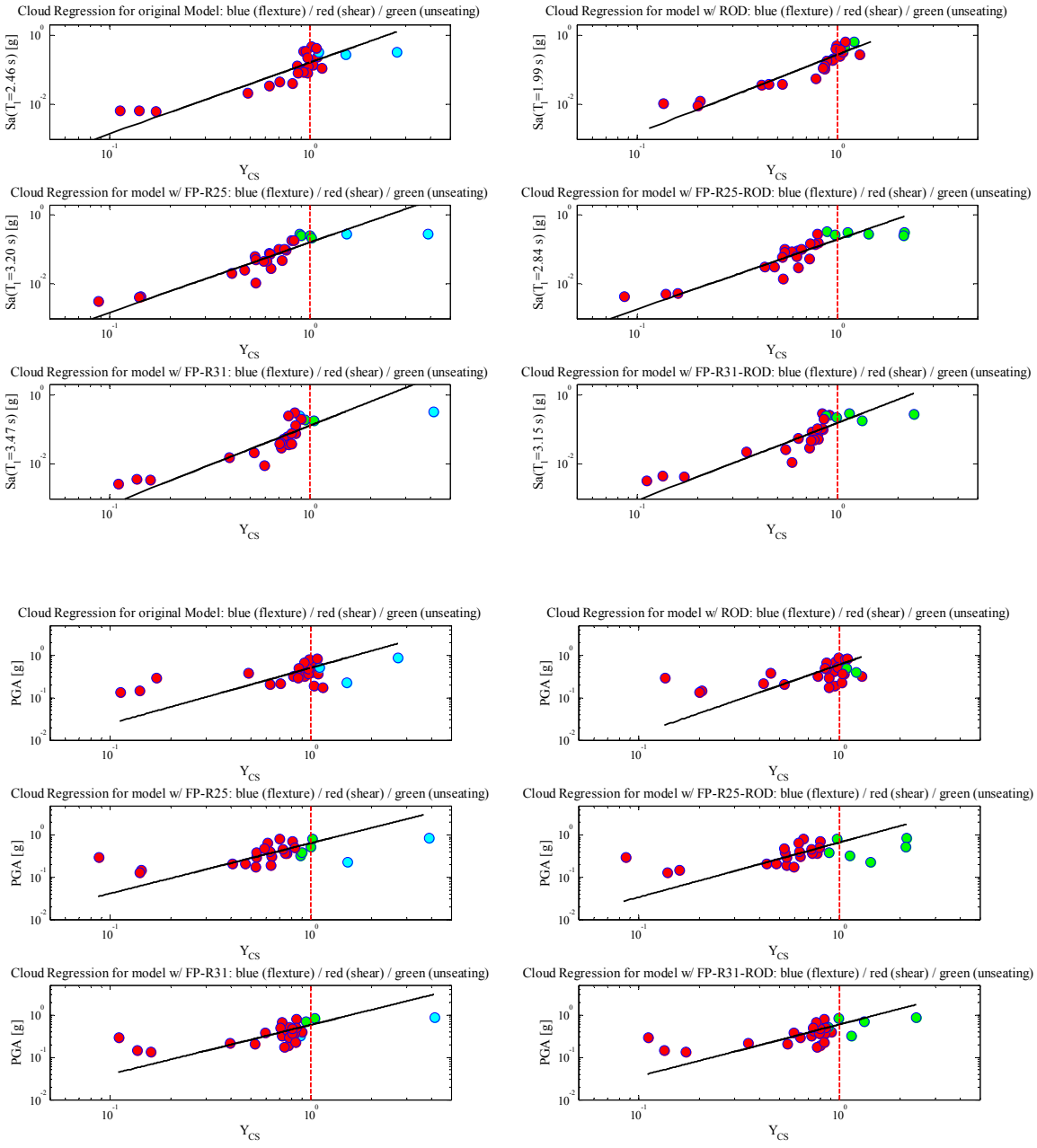
Cloud Regression for original Model: blue (flexture) / red (shear) / green (unseating)
Sa(T_I=2.46 s) [g]
Y_CS
Cloud Regression for model w/ ROD: blue (flexture) / red (shear) / green (unseating)
Sa(T_I=1.99 s) [g]
Y_CS
Cloud Regression for model w/ FP-R25: blue (flexture) / red (shear) / green (unseating)
Sa(T_I=3.20 s) [g]
Y_CS
Cloud Regression for model w/ FP-R25-ROD: blue (flexture) / red (shear) / green (unseating)
Sa(T_I=2.84 s) [g]
Y_CS
Cloud Regression for model w/ FP-R31: blue (flexture) / red (shear) / green (unseating)
Sa(T_I=3.47 s) [g]
Y_CS
Cloud Regression for model w/ FP-R31-ROD: blue (flexture) / red (shear) / green (unseating)
Sa(T_I=3.15 s) [g]
Y_CS
Cloud Regression for original Model: blue (flexture) / red (shear) / green (unseating)
PGA [g]
Y_CS
Cloud Regression for model w/ ROD: blue (flexture) / red (shear) / green (unseating)
PGA [g]
Y_CS
Cloud Regression for model w/ FP-R25: blue (flexture) / red (shear) / green (unseating)
PGA [g]
Y_CS
Cloud Regression for model w/ FP-R25-ROD: blue (flexture) / red (shear) / green (unseating)
PGA [g]
Y_CS
Cloud Regression for model w/ FP-R31: blue (flexture) / red (shear) / green (unseating)
PGA [g]
Y_CS
Cloud Regression for model w/ FP-R31-ROD: blue (flexture) / red (shear) / green (unseating)
PGA [g]
Y_CS

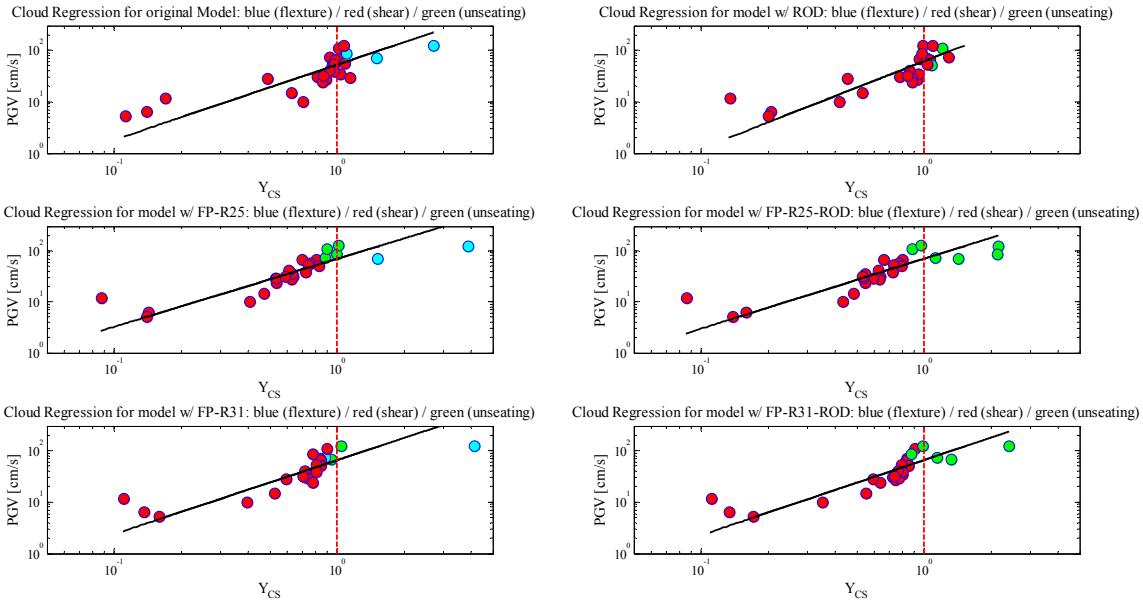

Figure 9: Cloud regression of different bridge models associated with the Collapse limit state (CS) based on the three different *IM*s considered

Step (2): Estimate Π_1 from Eq. (13) by convolving the fragility of the intact structure and the hazard λ_{IM}, for both limit states and different *IM* scenarios. Subsequently, $\{\Pi_{n,\mathbf{R}}|n=1{:}N_{ce}\}$ is evaluated directly from Eq. (17) by substituting $\Pi_{j+1}=\Pi_1$ as defined in Section 2.4. The repair times, denoted as τ, associated with alternative limit states are outlined in Table 6.

Limit state, *LS*	Repair time, τ [year]
Damage	1/2
collapse	1

Table 6: Repair time for alternative limit states

Step (3): Calculate the limit state probability by two different methodology:

(a) Directly substituting the probability Π_1 into Eq. (12) which is addressed as the *Standard method* for calculating the limit state exceedance probability in a given time interval. It is denoted as $P(LS|\tau=0,\mathbf{I}_1)$ and expressed by Eq. (14) (see Section 2.3).

(b) Calculating $\Pi_{2,\mathrm{R}}$ from Eq. (17) by substituting $n=2$, and subsequently set $\Pi=\Pi_{2,\mathrm{R}}$ in Eq. (12) as noted in Section 2.4. The limit state probability is addressed as **R** *decision* and denoted as $P(LS|\tau,\mathbf{I}_1)$.

Fig. 10 and Fig. 11 reveal the variation in $P(LS|\tau=0,\mathbf{I}_1)$ and $P(LS|\tau,\mathbf{I}_1)$ for both limit states given the desired *IM*s and given the time interval up to 100 years. It can be seen that by consideration of **R** *decision*, the time-dependent limit states will be fairly lower than those estimated by the *Standard method*. Moreover, the ordering of the limit state probabilities given *IM*s $Sa(T_1)$ and *PGV* reveal similar trend among both limit states as well as different limit state probability models. It is concluded that the retrofit strategies FP-R25, and FP-R25-ROD have

the lowest exceedance probabilities. However, this result cannot be clearly reported from those curves that correspond to the intensity *PGA*.

3.9 Calculating the Expected Life-Cycle Cost

The expected cost in the life-time of the bridge infrastructure is calculated for the five retrofit options described in Table 1 using Eq. (18). The initial costs C_0, which are composed of the initial cost of the construction (see [39, 40]) plus the cost of the desired retrofit upgrading [41], are tabulated in Table 7 for various retrofit options. The cost of maintenance C_M is calculated with reference to Eq. (20), where the constant annual maintenance cost C_m is also tabulated in Table 7.

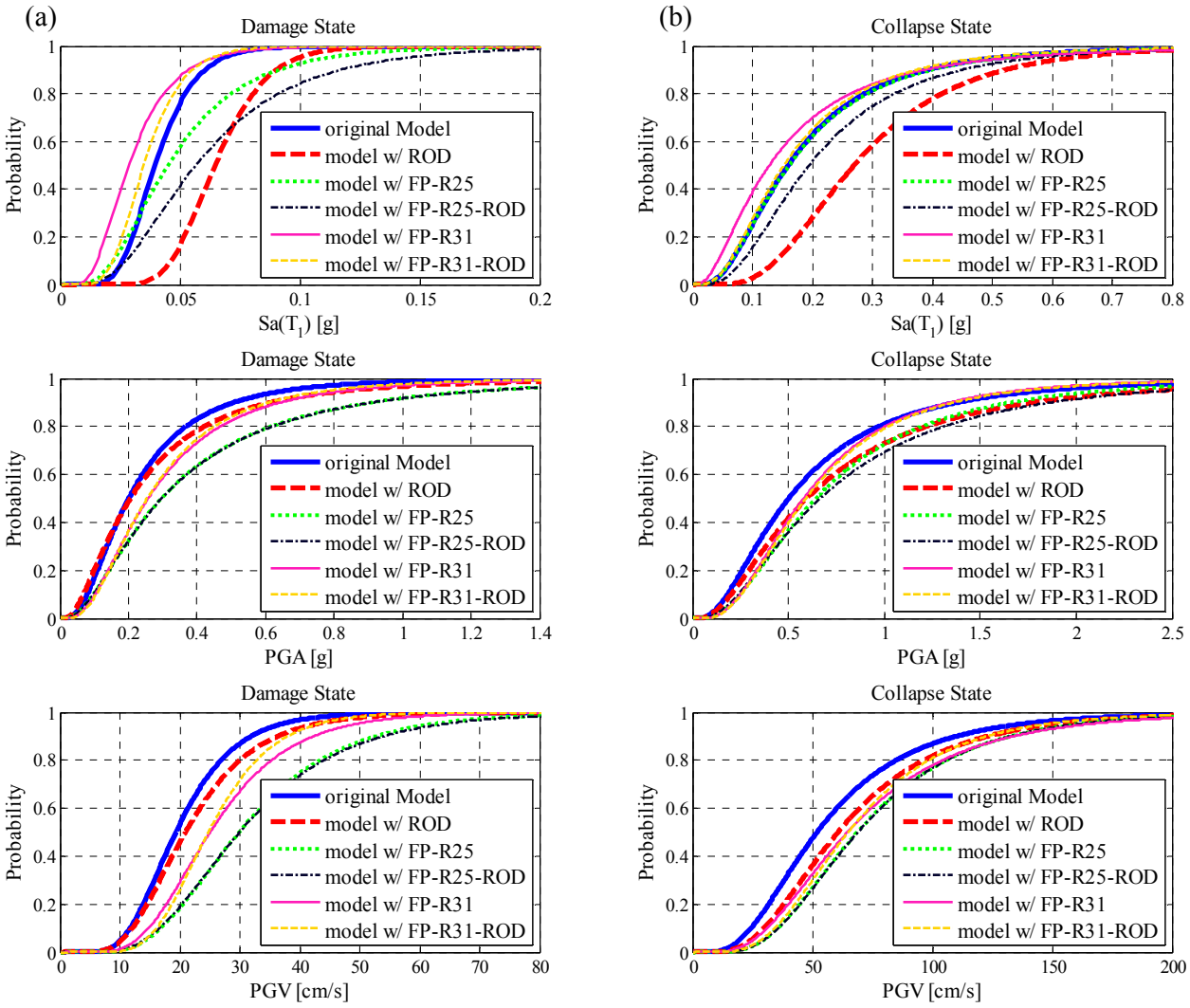

Figure 10: The fragility curves of various retrofit options based on desired *IM*s for (a) Damage and (b) collapse limit states

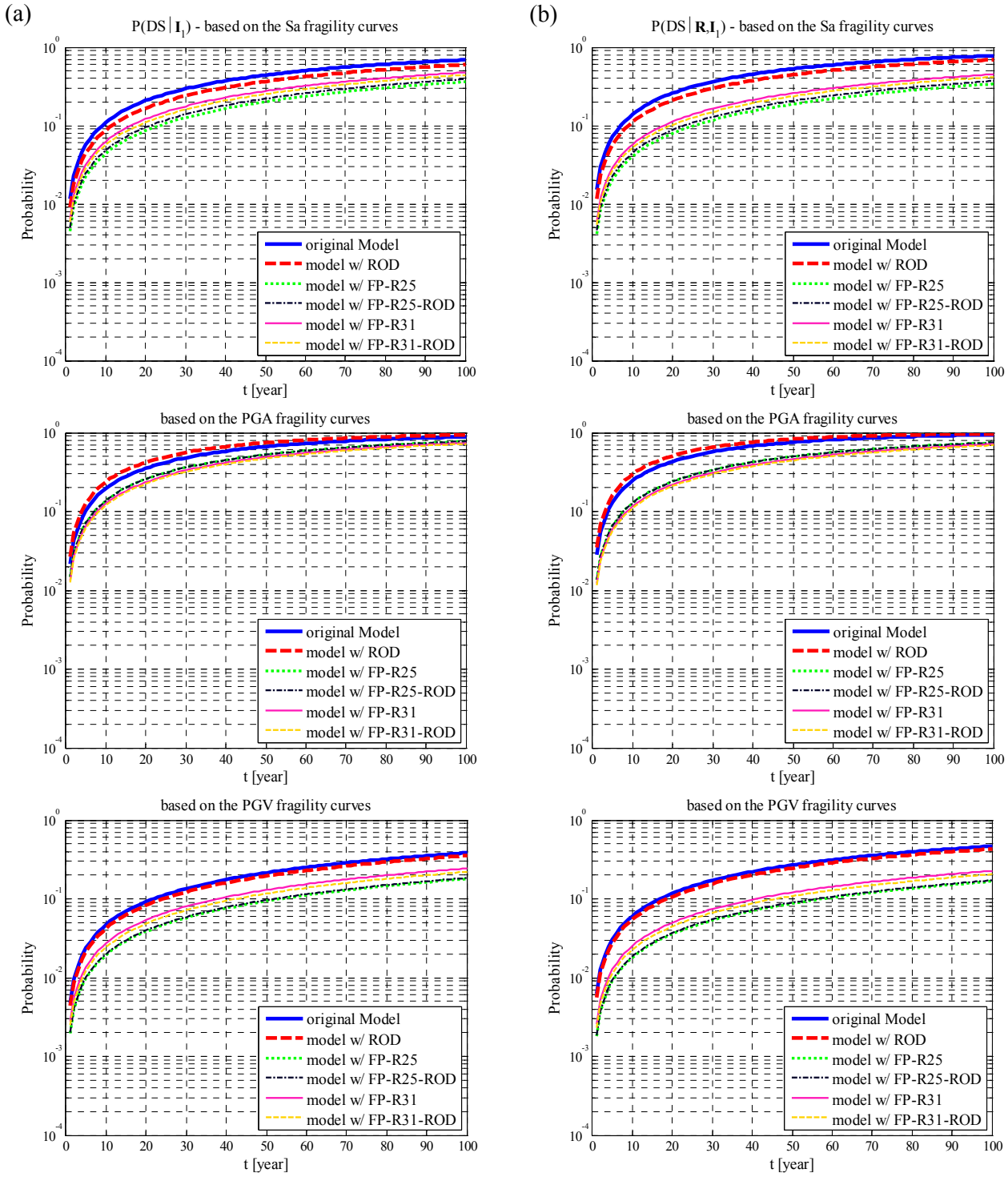

Figure 10: The time-dependent limit state probabilities for *Damage LS* (DS) for the case-study bridge with various retrofit schemes based on (a) *Standard method* - $P(LS|\tau=0,\mathbf{I}_1)$, (b) **R** *decision* - $P(LS|\tau,\mathbf{I}_1)$

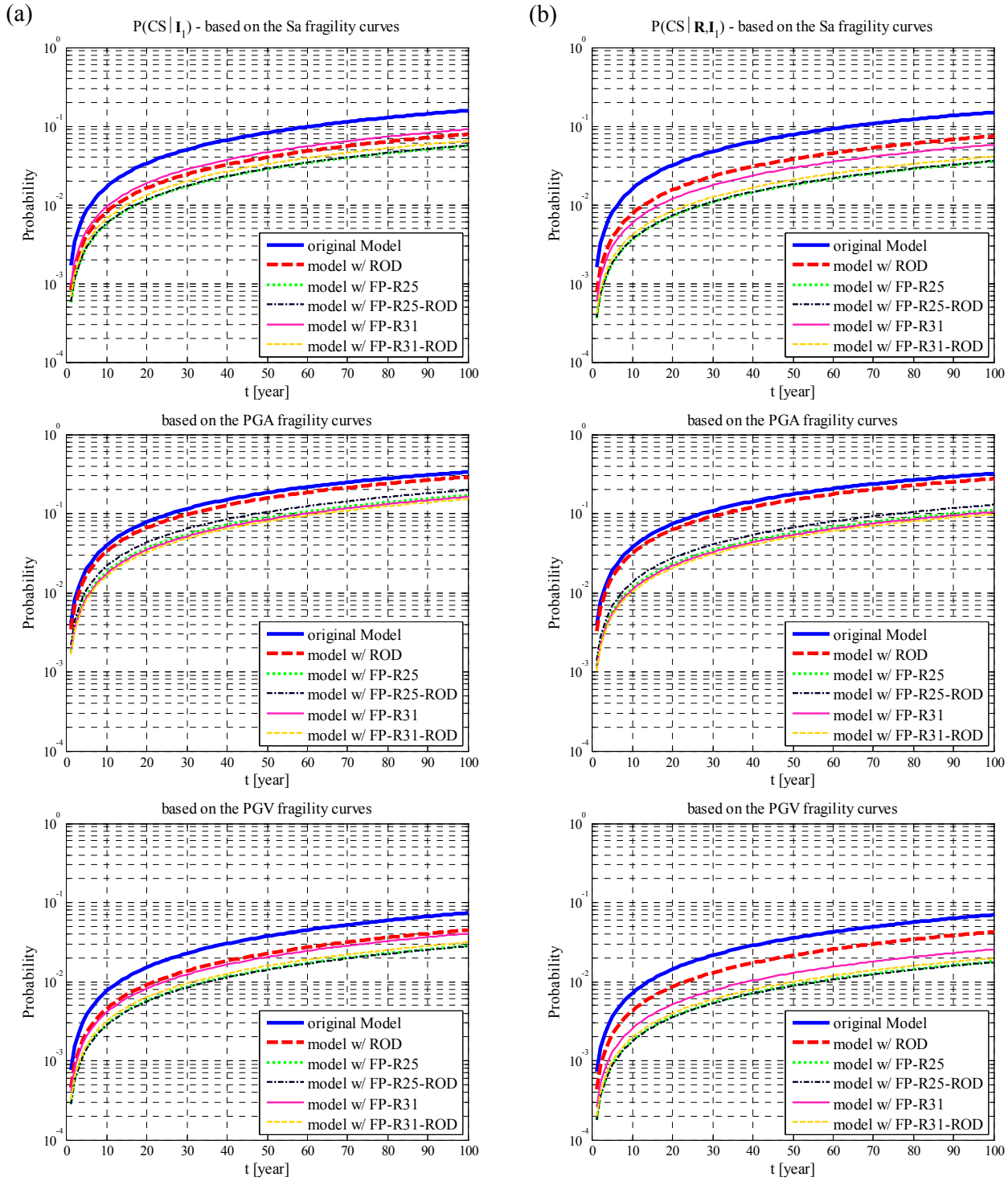

Figure 11: The time-dependent limit state probabilities for *Collapse LS* (CS) for the case-study bridge with various retrofit schemes based on (a) *Standard method* - $P(LS|\tau=0,\mathbf{I}_1)$, (b) **R** *decision* - $P(LS|\tau,\mathbf{I}_1)$

The repair/replacement cost C_R is calculated by using Eq. (19). Accordingly, LSC_{ls} where ls=1:N_{LS}=2, is the annual expected cost of restoring the infrastructure from the lsth limit state LS_{ls} back to its intact state including eventual loss of revenue due to downtime for repair operations. This expression is calculated herein as follows:

$$LSC_{ls} = DTC \cdot e^{-\lambda_d \tau} + RC_{ls} \tag{31}$$

where DTC is the annual cost of downtime outlined in Table 7, $\exp(-\lambda_d \tau)$ denotes the change in the monetary-based evaluations within the repair time where λ_d=0.05; RC_{ls} is the replacement cost associated with desired lsth limit state, ls=1:N_{LS}=2, and tabulated in Table 7; they are extracted from updated data calculated in [39, 40] and considered the same through different retrofit strategies.

Retrofit Option	C_0 ($\times 10^6$, €)	DTC ($\times 10^6$, €/year)	RC_{DS} ($\times 10^6$, €/year)	RC_{CS} ($\times 10^6$, €/year)	C_m ($\times C_0$, €/year)
Original Model	4.906	1	0.44	7.10	0.01
ROD	5.004	1	0.44	7.10	0.01
FP-R25	5.072	1	0.44	7.10	0.01
FP-R25-ROD	5.170	1	0.44	7.10	0.01
FP-R31	5.118	1	0.44	7.10	0.01
FP-R31-ROD	5.216	1	0.44	7.10	0.01

Table 7: Life-cycle cost analysis parameters

With reference to Eq. (19), the probability $P(LS_{ls}|[t,t+1],\mathbf{I}_1)$ is the limit state time-dependent probability in 1-year as a function of time t and for the lsth limit state, LS_{ls}, which is evaluated by using Eq. (8). However, in case of using the closed-from expression in Eq. (12) for time-dependent limit state probability, the following expression can simply be derived:

$$P\left(LS\,|\,[t,t+1],\mathbf{I}_1\right) = \frac{\mathrm{d}}{\mathrm{d}t}\left[1-\exp\left(-\Pi\,\nu t\right)\right]\cdot\left(\Delta t = 1\right) = \Pi\,\nu\exp\left(-\Pi\,\nu t\right) \tag{32}$$

Fig. 12 and Fig. 13 illustrate the resulting annual time-dependent limit state probabilities $P(LS_{ls}|[t,t+1],\mathbf{I}_1)$ for ls=1:2 given the desired *IM*s and given the time interval up to 100 years. Each figure reveals the annual exceedance probabilities in the *Standard method* (i.e. extracting $P(LS_{ls}|[t,t+1],\mathbf{I}_1)$ from $P(LS|\tau=0,\mathbf{I}_1)$ in Eq. 8) as well as considering the **R** *decision* by calculating $P(LS_{ls}|[t,t+1],\mathbf{R},\mathbf{I}_1)$ from $P(LS|\tau,\mathbf{I}_1)$.

In order to have a point of comparison, two threshold levels of 10% and 5% exceedance probability in 50 year are assigned to DS and CS, respectively, as shown by cyan bold line in Fig. 12 and Fig. 13. Thus, the admissible annual exceedance probability P_{adm} will become:

$$P_{adm,DS} = \lambda_{adm,DS}\cdot\exp\left(-\lambda_{adm,DS}\cdot t\right) = \left(2.1\times10^{-3}\right)\cdot\exp\left(-2.1\times10^{-3}\cdot t\right) \tag{33}$$

$$P_{adm,CS} = \lambda_{adm,CS}\cdot\exp\left(-\lambda_{adm,CS}\cdot t\right) = \left(1\times10^{-3}\right)\cdot\exp\left(-1\times10^{-3}\cdot t\right) \tag{34}$$

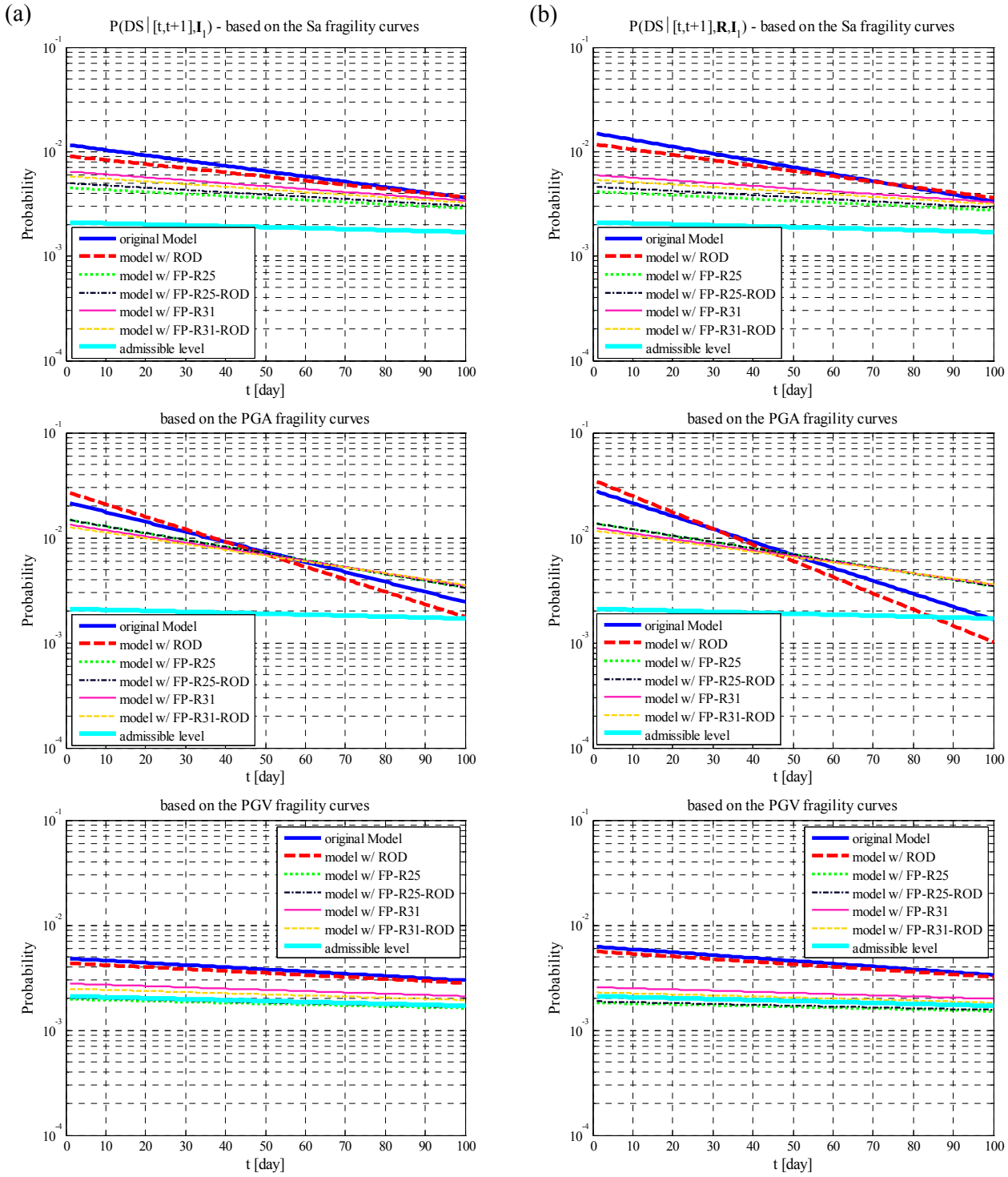

Figure 12: The *Damage LS* exceedance probability in 1-year as a function of time *t* for the case-study bridge with various retrofit schemes based on (a) *Standard method*, (b) **R** *decision*

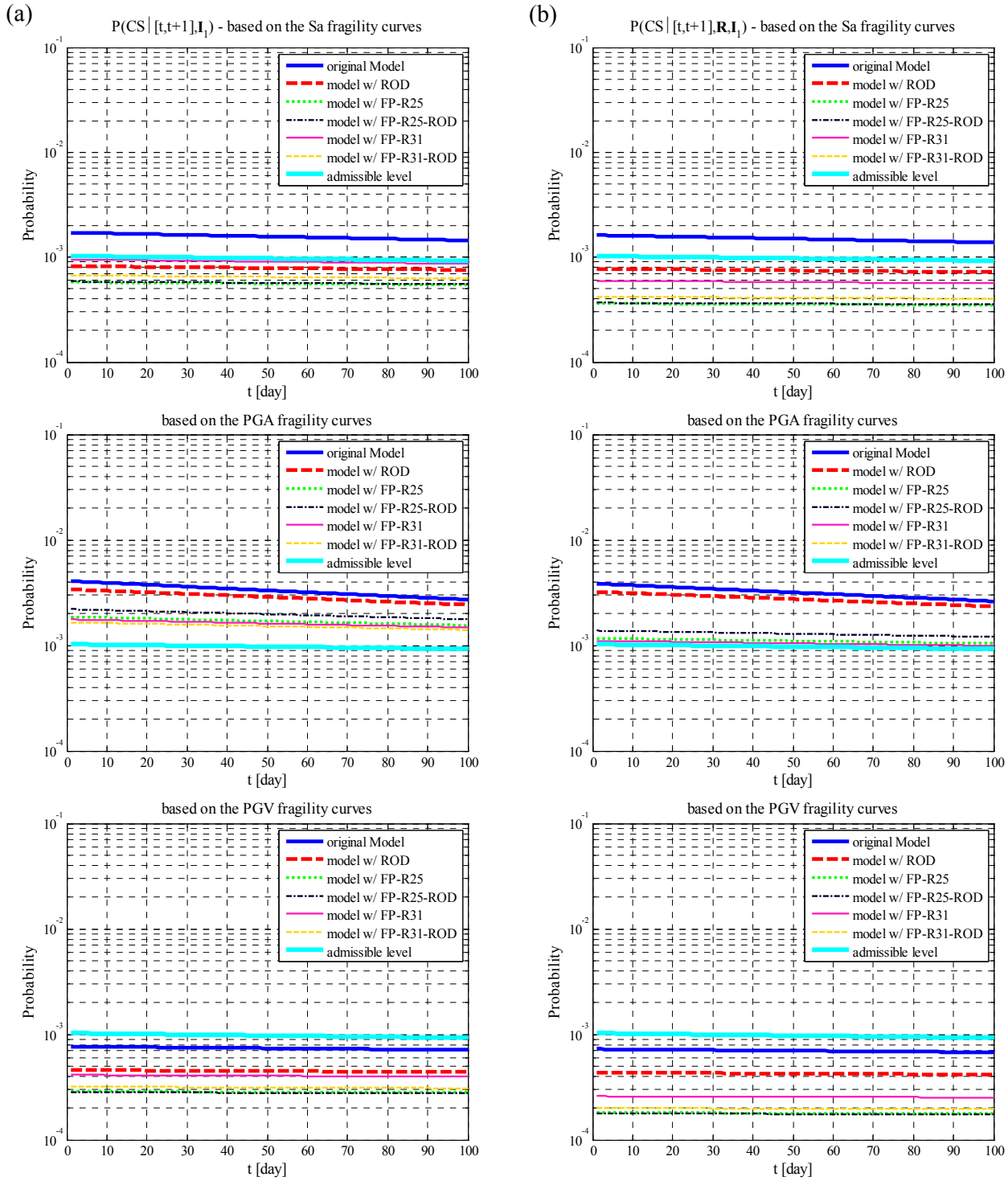

Figure 13: The *Collapse LS* exceedance probability in 1-year as a function of time *t* for the case-study bridge with various retro-fit schemes based on (a) *Standard method*, (b) **R** *decision*

It can be seen the by maintaining the **R** *decision*, the annual limit states probabilities are to some extend different with respect to the *Standard method*; moreover, the differences are more apparent compared to those revealed between $P(LS|\tau=0,\mathbf{I}_1)$ and $P(LS|\tau,\mathbf{I}_1)$ in Fig. 10 and Fig. 11. In addition, the outcomes of annual exceedance probability for CS based on *PGA* as the desired *IM* imply conservative decisions where the probability is higher than the admissible level even for the bridge with different retrofit strategies. The opposite conclusion will be extracted from those based on *PGV* as the desired *IM* where even the original infrastructure lies below the admissible level. However, the annual exccedance probabilities based on $Sa(T_1)$ denote that the original infrastructure is above the admissible level while the alternative retrofit strategies put the infrastructure below the admissible level. Since alternative *IM*s result in different decisions regarding the safety checking which directly affect the life-cycle cost assessment, their selection requires more detailed study.

In terms of life-cycle cost, Fig. 14 demonstrates the resulting expected life-cycle cost for alternative retrofit decisions based on using the *Standard method* or taking the **R** *decision*. It can be observed that:

(a) Based on both methods (i.e. *Standard* and **R** *decision*), the expected life-cycle costs for different retrofit options given the *PGV* as the desired *IM* does not reveal any enhancement in using alternative retrofit options. Hence, in terms of life-cycle cost assessment, the use of this *IM* requires more detailed studies (this conclusion was also drawn in the previous paragraph). However, the expected life-cycle costs given *PGA* or $Sa(T_1)$ reveal that the option FP-R25 (see Table 1) offers the lowest life-cycle cost while renders the bridge infrastructure competitively more reliable for the collapse limit state (see Fig. 13).

(b) Although the FP-R25 options are more expensive in the early stage of life time of the bridge infrastructure, it can be seen that after around 10-20 years (depends on the kind of *IM* for investigation), its corresponding expected cost fall beneath the other retrofit options. On the other hand, the retrofit option FP-R25-ROD has similar costs; however, it will decisively become the more expensive compared to FP-R25 as the time pass.

(c) The distinction between the expected costs of different retrofit options is more apparent while taking into account the repair time τ (i.e. using **R** *decision* with the limit state exceedance probability $P(LS|\tau,\mathbf{I}_1)$) compared to the *Standard method*, which assumes that $\tau=0$. Furthermore, the selection of *IM* affects the decisions regarding the life-cycle cost which requires more detailed studies.

(d) Taking the advantage that the *Standard method* is more convenient in its use, and knowing that it informs the same decision regarding life-cycle costs, it can be used in case of rapid screening among various retrofit options in terms of their life-cycle costs.

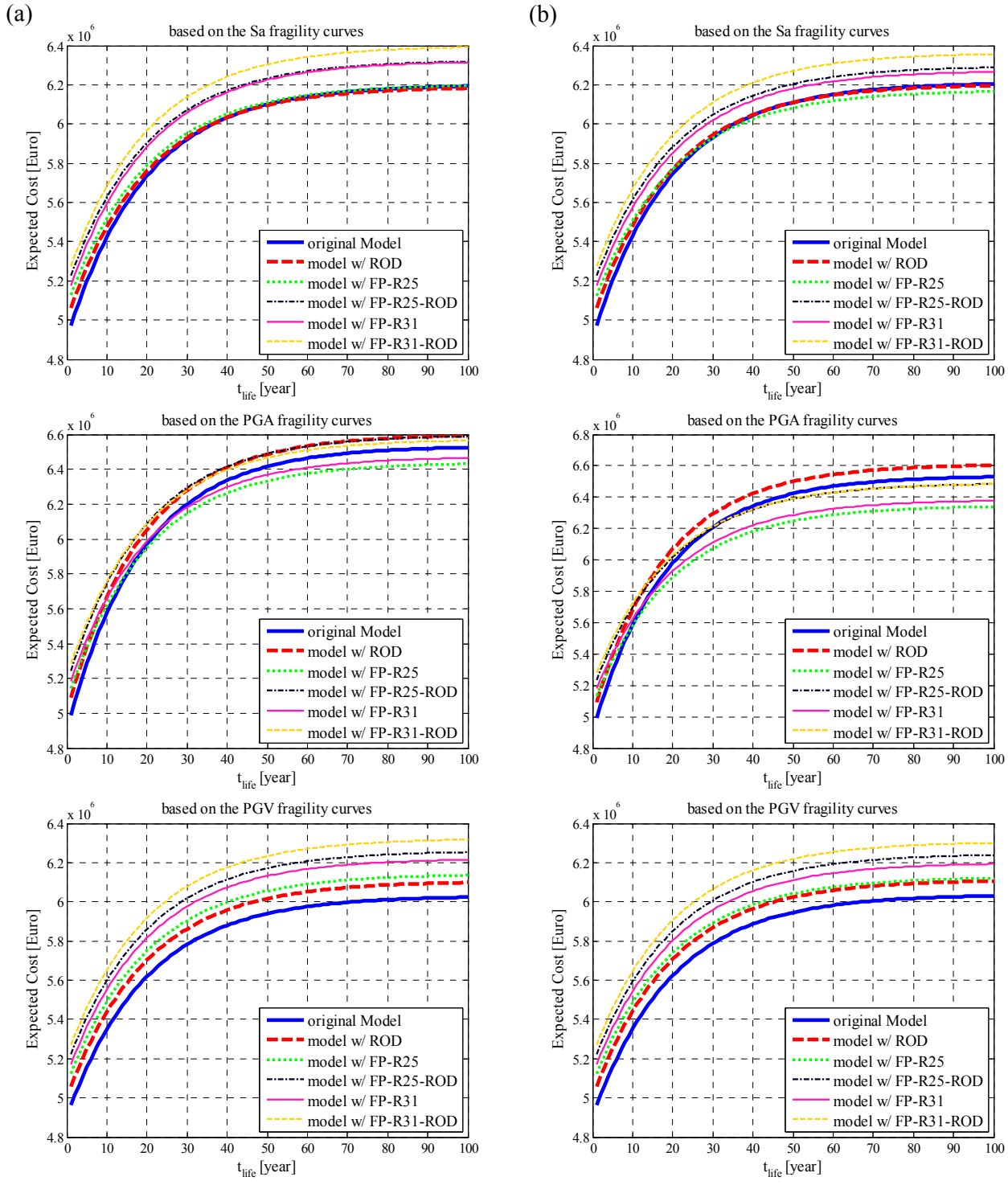

Figure 14: The expected life-cycle cost for alternative retrofit options (a) *Standard method*, (b) **R** *decision*

4 CONCLUSION

- A procedure is presented for retrofit decision-making based on life cycle criteria subjected to safety constraints. It can be effectively used for screening among various proposed retrofit strategies.
- Based on the assumption that a bridge is immediately subjected to repair operations after a major earthquake event, the finite repair time is considered in the life-cycle cost evaluation. This has been done by implementing a procedure developed by the authors for calculating the limit state exceedance probability taking into account the effect of cumulative damage due to a sequence of back-to-back seismic events. In particular, a simplified closed-form analytical expression for the limit state probabilities based on the fragility of intact infrastructure is employed.
- The time-dependent limit state probabilities are then used to calculate the expected life-cycle cost taking into account the total initial construction costs, down time, repair/replacement costs, and regular maintenance costs.
- This methodology is used as a decision-making tool for retrofit design of an existing RC bridge infrastructure in south Italy. The expected life cycle is calculated for the existing bridge (original model), and 5 different retrofit strategies. It is demonstrated that the Friction Pendulum isolator with effective radius of concave sliding surface equal to 2.5 m and a Coulomb friction of 2% (denoted as FP-R25) is the option that leads to the least expected life cycle cost. Although it is among the most expensive options in terms of installation costs, the corresponding expected cost falls beneath the other retrofit options after a certain amount of time.
- Alternative sufficient intensity measures (*IM*s) result in different decisions regarding the safety checking which directly affect the life-cycle cost assessment. Thus, their selection requires more detailed study.

The proposed methodology has its limitations:

- The effect of aging is not considered in the calculation of the limit state probabilities and the expected life cycle costs.
- The effect of cumulative damage is approximated by a simplified closed-form equation and based on the fragility of the intact bridge. That is, no back-to-back analyses are performed.
- The 3D model of the bridge infrastructure is subjected to ground-motion records in its longitudinal direction.
- The spatial variability in ground motion is not considered.
- The soil-structure interaction is not considered.

APPENDIX

The general procedure for calculating the set of event-dependent fragilities $\{\pi_n(x)|n=1{:}N_{ce}\}$ (entered in Eq. 6) in this study is described as follows (see also [6-9]):

1. Construct the nonlinear model of the desired structure.
2. Select a suite of ground motion records.
3. Clone (repeat) each record in the set n times (n=1:N_{ce}) to construct a sequence.
4. Perform a finite element nonlinear dynamic analysis of the representative model of structure by subjecting it to the suite of constructed sequences comprising of the cloned ground motions (previous step). However, exclude those sequences, in which the limit state first-excursion has already taken place in their previous (n-1) events, from the suite of sequences.
5. For each sequence, calculate the time- and history-dependent performance variable $Y_{LS}^{(n)}$ that tends to reflect and to conditionally isolate the effect of the nth event on the desired structure [9]:

$$Y_{LS}^{(n)} = \frac{D_{\max}^{(n)} - D_r^{(n-1)}}{C_{LS} - D_r^{(n-1)}} \tag{A.1}$$

   where $D_{\max}^{(n)}$ is the maximum demand due to the nth event in the sequence; $D_r^{(n\text{-}1)}$ is the residual demand corresponding to the sequence of (n-1) events; C_{LS} is the limit state capacity of the (intact) structure. The term $Y_{LS}^{(n)}$ can be regarded as the ratio of maximum demand increment due to the nth event divided by the reduced capacity right after the sequence of (n-1) events. Needless to say that at the onset of the limit state, $Y_{LS}^{(n)}$=1.
6. For each sequence, register the pair of cloud data [$IM^{(n)}$, $Y_{LS}^{(n)}$] corresponding to nth event.
7. Modify the cloud analysis data at nth step (if required). This issue can be addressed by paying attention to the range of $Y_{LS}^{(n)}$ values, which should manage to especially cover the values greater than or equal to unity (see general notes on cloud analysis while using Y_{LS} in [27]). This modification can be accomplished by deliberately substituting the existing nth cloned record in the sequence with the one that has been excluded (see Step 4) while maintaining $Y_{LS}^{(n)} \geq 1$.
8. Let $N_{gm}(n)$ be the number of ground motions in the suite of records at nth step, carry out a logarithmic linear regression on $N_{gm}(n)$ cloud data by assuming that the conditional distribution of $Y_{LS}^{(n)}$ given a level of $IM^{(n)}$=x is described by a lognormal distribution ([29, 42, 43]); thus, the fragility term $\pi_n(x)$ can be expressed as:

$$\pi_n(x) = P\left(C_n \mid x, \mathbf{I}_2\right) = 1 - \Phi\left(\frac{-\ln \eta_{Y_{LS}|IM}^{(n)}(x)}{\beta_{Y_{LS}|IM}^{(n)}}\right) \tag{A.2}$$

   where Φ is the standardized Gaussian cumulative distribution function (CDF); $\eta_{YLS|IM}^{(n)}$ and $\beta_{YLS|IM}^{(n)}$ are conditional median and standard deviation (dispersion) of the natural logarithm of $Y_{LS}^{(n)}$ given spectral acceleration and given that the structure has already been subjected to n events. The median and dispersion can be calculated as [40]:

$$\ln \eta_{Y_{LS}|IM}^{(n)}(x) = \ln a + b \ln(x), \quad \beta_{Y_{LS}|IM}^{(n)} = \sqrt{\frac{\sum_{i=1}^{N_{gm}(n)} \left[\ln\left(Y_{LS,i}^{(n)} / a \cdot (IM_i^{(n)})^b\right)\right]^2}{N_{gm}(n) - 2}} \tag{A.3}$$

   where ln$a$ and b are the coefficients of the logarithmic linear regression.
9. Repeat steps 3-8 for the same suite of ground motion records until n=N_{ce}.

AKNOWLEDGEMENT

This work was supported in part by project STRIT (Strumenti e Tecnologie per la gestione del Rischio delle Infrastrutture di Trasporto). This support is gratefully acknowledged. Any opinions, findings, and conclusions or recommendations expressed in this material are those of the authors and do not necessarily reflect those of the sponsors. The authors would like to gratefully acknowledge Dr. Luigi Di Sarno and Jonatan Picariello for providing the initial information of the bridge infrastructure and helping in the OpenSees modeling of the bridge. Finally, the authors would like to gratefully acknowledge Dr. Luigi Petti and Alessio Lodato for providing the information for different retrofit options of the bridge.

REFERENCES

[1] Y.K.Wen, Reliability and performance-based design. *Structure Safety*, **23**(4), 407-428, 2001.

[2] M.H. Faber, R. Rackwitz, Sustainable decision making in Civil Engineering. *Structural Engineering International*, **14**(3), 237-242, 2004

[3] K.A. Porter, A.S. Kiremidjian, J.S. LeGrue, Assembly-based vulnerability of buildings and its use in performance evaluation. *Earthquake Spectra*, **17**(2), 291-312, 2001

[4] P. Franchin, P.E. Pinto, M.IJ. Schotanus, Seismic loss estimation by efficient simulation. *Journal of Earthquake Engineering*, **10**(1):31-44, 2006

[5] C.A. Goulet, C.B. Haselton, J. Mitrani-Reiser, J.L. Beck, G.G. DeierLein, K.A. Porter, J.P. Stewart, Evaluation of the seismic performance of a code-conforming reinforced concrete frame building - From seismic hazard to collapse safety and economic losses. *Earthquake Engineering and Structural Dynamics*, **36**(13), 1973-1997, 2007.

[6] F. Jalayer, D. Asprone, A. Prota, G. Manfredi, Multi-hazard upgrade decision making for critical infrastructure based on life-cycle cost criteria. *Earthquake Engineering and Structural Dynamics*, **40**(10), 1163-1179, 2011.

[7] F. Jalayer, D. Asprone, R. Chiodi, A. Prota, G. Manfredi, Seismic Retrofit Decision-Making based on Life Cycle Cost Criteria. *15th Word Conference on Earthquake Engineering (15WCEE)*, Lisbon, Portugal, 2012.

[8] F. Jalayer, D. Asprone, A. Prota, G. Manfredi, A decision support system for post-earthquake reliability assessment of structures subjected to aftershocks: an application to L'Aquila earthquake, 2009. *Bulletin of Earthquake Engineering*, **9**(4), 997-1014, 2011.

[9] H. Ebrahimian, F. Jalayer, D. Asprone, A.M. Lombardi, W. Marzocchi, A. Prota, G. Manfredi, A performance-based framework for adaptive seismic aftershock risk assessment, *Earthquake Engineering and Structural Dynamics*, **43**(14), 2179-2197, 2014.

[10] F. Jalayer, H. Ebrahimian, G. Manfredi, Towards quantifying the effect of aftershocks in seismic risk assessment. *12th International Conference on Applications of Statistics and Probability in Civil Engineering (ICASP12)*, Vancouver, Canada, July 12-15, 2015.

[11] J.R. Benjamin, C.A. Cornell. *Probability, statistics and decision for civil engineers*, McGraw Hill, 684pp, 1970.

[12] D. Cardone, P. Giuseppe, S. Salvatore, A performance-based adaptive methodology for the seismic evaluation of multi-span simply supported deck bridges. *Bulletin of Earthquake Engineering*, **9**(5), 1463-1498, 2011.

[13] ASPI (AutoStrade Per l'Italia S.p.a), *S.A.M.O.A.: Survey, Auscultation and Maintenance of Bridges*, Autostrade per l'Italia S.p.a., Rome, 1992.

[14] OpenSees. *Open system for earthquake engineering simulation*. Pacific Earthquake Engineering Research Center, (PEER), April 2015. (Available from: http://opensees.berkeley.edu).

[15] M.H. Scott, G.L. Fenves, Plastic hinge integration methods for force-based beam–column elements. *Journal of Structural Engineering*, **132**(2), 244-252, 2006.

[16] CEN (Comité Européen de Normalisation), *Eurocode 8: Design of structures for earthquake resistance - Part 3: Assessment and retrofitting of buildings*. EN 1998-3, CEN, Bruxels, 2005.

[17] CEN (Comité Européen de Normalisation), *Eurocode 8: Design of structures for earthquake resistance - Part 2: Bridges*. EN 1998-2, CEN, Bruxels, 2005.

[18] M.J.N. Priestley, F. Seible, G.M. Calvi, *Seismic Design and Retrofit of Bridges*, John Wiley & Sons, Inc., New York, 1996.

[19] P. Kaviani, F. Zareian, E. Taciroglu, *Performance-Based Seismic Assessment of Skewed Bridges*, *Report PEER 2014/01*, Pacific Earthquake Engineering Research Center, University of California, Berkeley, CA, 2014.

[20] J.B. Mander, M.J.N. Priestley, R. Park, Theoretical stress-strain model for confined concrete. *Journal of structural* engineering, **114**(8), 1804-1826, 1988

[21] A. Aviram, K.R. Mackie, B. Stojadinovic, *Guidelines for nonlinear analysis of bridge structures in California*, *Report PEER 2008/3*, Pacific Earthquake Engineering Research Center, University of California, Berkeley, CA, 2008.

[22] R.W. Clough, J. Penzien, *Dynamics of structures*, *2nd Edition*, New York: McGraw-Hill, Inc., 1994.

[23] L. Petti, A. Lodato, A. Mammone, Reliability analysis of seismic isolation in retrofitting of simply supported bridges. *Advances in Civil and Infrastructure Engineering*, Vietri sul Mare, Italy, June 12-13, 2015.

[24] L. Petti, A. Lodato, A. Mammone, Il miglioramento sismico di ponti a travata semplicemente appoggiata mediante isolamento sismico. *XVI Convegno ANIDIS, L'Ingegneria Sismica in Italia*, L'Aquila, Italia, settembre 13-17, 2015 (in Italian).

[25] B. Borzi, P. Ceresa, P. Franchin, F. Noto, G.M. Calvi, P.E. Pinto, Seismic Vulnerability of the Italian Roadway Bridge Stock. *Earthquake Spectra*, In-Press, 2014, DOI 10.1193/070413EQS190M.

[26] CEN (Comité Européen de Normalisation), *Eurocode 8: design of structures for earthquake resistance - Part 1: General rules, seismic actions and rules for buildings*. EN 1998-1 CEN Brussels, 2004.

[27] T. Isaković, L. Bevc, M. Fischinger, Modeling the cyclic flexural and shear response of the RC hollow box columns of an existing viaduct. *Journal of Earthquake Engineering*, **12**(7), 1120-1138, 2008

[28] F. Jalayer, P. Franchin, P.E. Pinto. A scalar damage measure for seismic reliability analysis of RC frames. *Earthquake Engineering and Structural Dynamics*, **36**(13), 2059-2079, 2007

[29] F. Jalayer, R. De Risi, G. Manfredi, Bayesian Cloud Analysis: efficient structural fragility assessment using linear regression. *Bulletin of Earthquake Engineering*, 13, 1183-1203, 2015.

[30] P. Franchin, P.E. Pinto, Allowing traffic over mainshock-damaged bridges. *Journal of Earthquake Engineering*, **13**(5), 585-599, 2009.

[31] T.D. Ancheta, R.B. Darragh, J.P. Stewart, E. Seyhan, W.J. Silva, B.S.-J. Chiou, K.E. Wooddell, R.W. Graves, A.R. Kottke, D.M. Boor, T. Kishida, J.L. Donahue, NGA-West2 Database. *Earthquake Spectra* **30**(3), 989-1005, 2014.

[32] S.K. Shahi, *A probabilistic framework to include the effects of near-fault directivity in seismic hazard assessment*. Dissertation, Stanford University, CA, 2013.

[33] Gruppo di Lavoro, 2004. *Redazione della mappa di pericolosità sismica prevista dall'Ordinanza PCM 3274 del 20 marzo 2003*. Rapporto Conclusivo per il Dipartimento della Protezione Civile, INGV, Milano-Roma, April 2004, 65 pp. + 5 appendixes (in Italian).

[34] MATHAZARD, *A program for seismic hazard analysis*, University of Rome, Italy, December 2000.

[35] F. Sabetta, A. Pugliese, Estimation of response spectra and simulation of nonstationary earthquake ground motions. *Bulletin of the Seismological Society of America*, **86**(2), 337-352, 1996.

[36] L. Elefante, F. Jalayer, I. Iervolino, G. Manfredi, Disaggregation-based response weighting scheme for seismic risk assessment of structures. *Soil Dynamics and Earthquake Engineering*, **30**(2), 1513-1527, 2010.

[37] F. Jalayer, J. Beck, F. Zareian, Analyzing the sufficiency of alternative scalar and vector intensity measures of ground shaking based on information theory. *Journal of Engineering Mechanics*, **138**(3), 307-316, 2011.

[38] H. Ebrahimian, F. Jalayer, A. Lucchini, F. Mollaioli, G. Manfredi, Preliminary ranking of alternative scalar and vector intensity measures of ground shaking. *Bulletin of Earthquake Engineering*, In-Press, 2015, DOI 10.1007/s10518-015-9755-9.

[39] A. Miano, F. Jalayer, R. De Risi, A. Prota, G. Manfredi, A case-study on scenario-based probabilistic seismic loss assessment for a portfolio of bridges. *12th International Conference on Applications of Statistics and Probability in Civil Engineering (ICASP12)*, Vancouver, Canada, July 12-15, 2015.

[40] A. Miano, F. Jalayer, R. De Risi, A. Prota, G. Manfredi, Bridge portfolio seismic loss assessment: simulation of the direct losses due to Irpinia 1980 earthquake, *Bulletin of Earthquake Engineering*, submitted, 2015.

[41] *Prezzi informative opere edili nella regione Abruzzo*, Direzione lavori pubblici ciclo idrico integrato difesa del suolo e della costa protezione civile, servizio tecnico regionale dei ll.pp., 2013 (in Italian).

[42] F. Jalayer, C.A. Cornell, *A Technical Framework for Probability-Based Demand and Capacity Factor Design (DCFD) Seismic Formats*, *Report PEER 2003/08*, , University of California, Berkeley, CA, 2003.

[43] F. Jalayer, C.A. Cornell, Alternative non-linear demand estimation methods for probability-based seismic assessments. *Earthquake Engineering and Structural Dynamics*, **38**(8), 951-972, 2009.